EXPERIMENTAL AND NUMERICAL STUDIES ON SUPERHIGH STRENGTHENING SINTERED LOW ALLOY STEELS FABRICATED BY METAL INJECTION MOLDING

ワン シャルジ ワン ハルン

https://doi.org/10.15017/1398373

EXPERIMENTAL AND NUMERICAL STUDIES ON SUPERHIGH STRENGTHENING SINTERED LOW ALLOY STEELS FABRICATED BY METAL INJECTION MOLDING

Doctoral Thesis
July 2013

Wan Sharuzi Wan Harun

Supervisor
Professor Dr. Hideshi Miura

Department of Mechanical Engineering
Graduate School of Engineering
Kyushu University

ABSTRACT

Metal injection molding (MIM) process is an advanced powder processing technique because of net shaping with shape complexity at low processing energy and 100 % material utilization. This study has been performed to clarify and to optimize the relationship between the mechanical properties and the microstructures for obtaining the superhigh strengthening sintered low alloy steels (Fe-Ni system) by using MIM process. The influence of nickel particle sizes, nickel content, and sintering conditions on the microstructure and mechanical properties of superhigh strengthened Fe-Ni steel compacts have been systematically investigated. As starting materials, the mixed elemental of carbonyl iron and water-atomized nickel powders were utilized. Tempered compact added 6 mass% fine nickel powder followed by sintering at 1250 ºC for 1 hour showed superhigh strength of 2040 MPa with elongation of 8.1 %, which was the best properties among reported data in P/M low alloy steels so far. These excellent mechanical properties is due to the fine heterogeneous microstructure consisted of nickel rich phase surrounded by a networks of tempered martensitic structures.

The mechanical properties of MIM compacts are highly dependent on two major factors; the porosity, and the microstructural morphology in the matrix. Both factors were cautiously considered in the present work. The porosity studies was carried out on 440C sintered steel, which was a high strength material with numerous pore contents. For the latter, the superhigh strengthened Fe-Ni steel compact, which is a primary alloy steel in this study was employed for microstructural studies on the matrix. Not only experimental work but also numerical simulation by finite element method was engaged to understand how these factors work.

440C steel compact has been purposely used as an example material to examine the pore factor. The utilization of 440C steel compact was due to homogeneous microstructure of matrix although contained many residual pores. The porosity study begins with experimental works, followed by numerical simulation for verification. The model demonstrated that tensile properties was enhanced at reduced pores and depreciated when the porosity was increased. Also, when mechanical properties of the

compacts with similar porosity level is compared, the pore factor can be disregarded due to their minimum influences. However, the pores became a major factor when comparing compacts of different porosity levels.

After the pore factor was successfully tested and evaluated, the effort had extended to the core focus of the present study. The effect of heterogeneous microstructure was treated in order to evaluate superhigh strengthened Fe-Ni steel compacts. Sintered density of all Fe-Ni steel compacts obtained in this study was 95-96 %, it means the porosity levels were about similar. Therefore, the pore factor has been simply omitted.

The microstructure of all superhigh strengthened Fe-Ni steel compacts have been consistently structured by heterogeneous condition. The microstructural heterogeneity aspects of the compact were changed by the characteristics of Ni powder, such as particle size, shape, and content, which play important roles in the deformation behavior. A complex network of higher Ni region which firmly bounded by the lower Ni region (matrix region) has been comprehensively observed.

The high ductility and high strength offered by the superhigh strengthened Fe-Ni steel compacts were probably also due to mechanically induced martensitic transformation that takes place during deformation. The material was initially metastable retained austenite, which was relatively ductile phase and the ductility was enhanced by the martensitic transformation-induced plasticity (TRIP) phenomenon. The high strength was due to the transformation of the soft austenite phase to the hard martensitic phase during the deformation as experimentally observed.

In order to understand how the microstructure results these high mechanical properties, finite element modeling based on the spatial distribution obtained experimentally was developed. Some parameters were prepared to control heterogeneity in the representative volume element. The simulated results were compared to experimentally obtained behavior, and showed good agreements. These capabilities of successful simulation of the actual microstructure by FEM resulted possibility to identify and design an optimum microstructure theoretically for Fe-Ni system.

TABLE OF CONTENTS

5. CONCLUSIONS AND FUTURE DIRECTIONS

CHAPTER 1

Introduction

1.1 BACKGROUND

1.1.1 Fe-Ni Steel Compacts by MIM

The excellent mechanical properties offered by superhigh strengthened Fe-Ni steel compacts have been widely known. Since then, numerous efforts have been put into placed by various researchers in order to have better explanations on the mechanics of strengthening Fe-Ni alloys system.

Especially, Miura et al. reported that most important point was not only the solid solution of Ni but also fine heterogeneity which consists of Ni rich phase surrounded by a network of tempered martensitic structure as schematically shown in Fig. 1.1 [1]. This heterogeneity resulted in good balance of strength and ductility. From their works, the best mechanical properties attained by tempered Fe-6Ni-0.5Mo-0.2Mn-0.4C using mixed elemental powders of carbonyl Fe and Ni, Mo, and Fe-25Mn were 1985 MPa tensile strength and 5 % elongation [2]. The Ni concentration profile obtained by electron probe microanalyzer (EPMA) found out that peaks and valleys of Ni content were dispersed throughout the mezzo heterogeneous microstructure matrix [1-3].
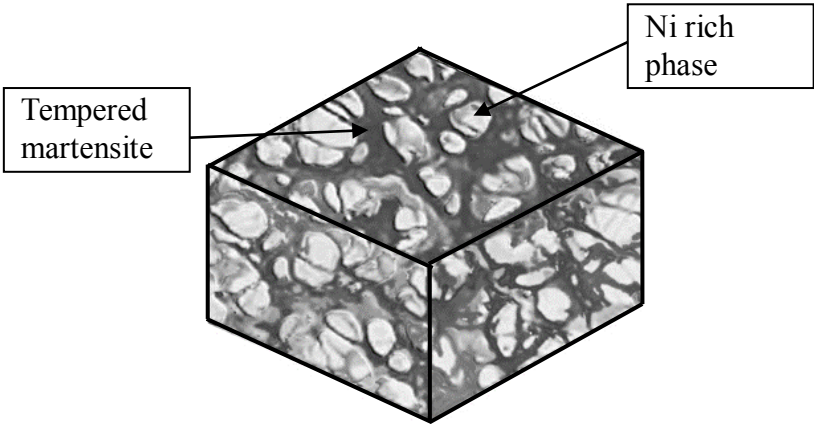
Fig. 1.1 Schematic diagram of 3D superhigh strengthened Fe-Ni steel microstructure where Ni phase surrounded by tempered martensite structure.

Furthermore, comparative studies for the effect of prealloyed and mixed elemental-based powders on the mechanical properties of AISI 4600 (Fe-2Ni-0.2Mn-0.5Mo-0.89C) and AISI 4100 (Fe-0.2Cr-2Mn-0.5Mo-0.89C) have been extensively investigated by Miura [4]. All prealloyed-based compacts exhibited homogeneous microstructure, while the microstructures of mixed elemental-based compacts were heterogeneous. However, as sintering temperature increases, the microstructure of mixed elemental-based compact became similar to that of prealloyed-based homogeneous compact. It is worth noting that all mechanical properties of mixed elemental-based compacts were found superior over the prealloyed-based compacts [4-5].

Until now, numerous interesting experimental data are available especially on heterogeneous nature of superhigh strengthened Fe-Ni steel compact microstructures by Miura [1-5] and other researchers [6-9]. However, there has been no attempts reported to numerically explain the strengthening mechanism of this distinctive heterogeneous structure. In this study, a FEM simulation work has been also implemented in order to gain better comprehensive understanding about the nature of heterogeneous microstructure of superhigh strengthened Fe-Ni steel compacts.

1.1.2 Microstructural Simulation

For design and development of high-performance materials using FEM modeling, it requires a thorough understanding and careful selection of factors that control a microstructure and its effect on mechanical properties. This is particularly challenging to make reliable numerical demonstration of the multiphase and heterogeneous nature of most high-performance alloy like Fe-Ni steel compacts. It is a complex problem to model and to predict the overall elastic-plastic response and local damage mechanisms in heterogeneous microstructure-based alloys, in particular in the metal injection molding (MIM) components [10-14].

For the compacts with heterogeneous microstructure, numerical modeling techniques, such as the finite element method (FEM), are often more effective than

mathematical modeling since the deformation and damage characteristics, particularly on a local scale, can be certainly revealed. In order to model the behavior of heterogeneous microstructure, assumption of simple geometry in a unit cell model is typically taken [15-17]. Unit cell models have been employed to model fracture, void nucleation, growth and coalescence of voids within a metallic matrix [15], and crack growth along the particle/matrix interface [18].

Another important aspect of the microstructure in a compact is the effect of spatial distribution of the alloy elements. The link between spatial distribution and mechanical behavior has not been modeled extensively [18-19]. Ghosh and co-workers [20-21] used a serial sectioning technique to obtain the spatial distribution of SiC particles, and quantified the spatial distribution by a tessellation scheme. Modeling of damage in the compact was conducted on two-dimensional (2D) sections by approximating the particle morphology as ellipsoids, so the deformation assumed a 2D stress state (plane stress, plane strain, or modified plane strain). A three-dimensional (3D) elastic Voronoi cell is also being developed [22], once again using ellipsoid particles. Boselli et al. [19] modeled the effect of crack growth using idealized 2D microstructures, consisting of circular disks embedded in a metal matrix. It was found that clustering had a significant effect on the local shielding and "anti-shielding" effects at the crack tip. Llorca and co-workers [18] modeled the effect of particle clustering on damage in metal matrix compacts. The particles, modeled as spheres, were incorporated with different degrees of clustering (as quantified by a radial distribution function). A similar modeling approach was taken by Bohm and co-workers [23-24].

In this study, the primary work was to discover interrelation between the heterogeneous distribution of Ni concentration throughout the matrix and the mechanical properties of superhigh strengthened Fe-Ni steel compacts. The work was accomplished experimentation followed by numerical simulation.

Before carrying out the simulation for heterogeneous microstructure, numerical simulation for pore structure was performed to check effectiveness of FEM simulation in the present work. It should be noted, for P/M parts that residual pores are usually

found in the compact. These residual pores could be a major unfavorable factor to mechanical properties if not appropriately considered. For working components manufactured by MIM process, maximum acceptable porosity level is 5 % [28,29,31,33]. Therefore, a preliminary studies which focused on the mechanical properties of the compacts containing pores was also performed. Since the porosity factor is a common issue for compacts, the work in this study begins dealing with the effect of pores on the mechanical properties of the compacts in the field of P/M or more specific in the MIM.

1.1.3 Steel Compact

As briefly mentioned in the previous section, the steel compacts fabricated by powder metallurgy (P/M) or metal injection molding (MIM) are typically characterized by residual pores after sintering, which quite detrimental to the mechanical properties of the compacts [25-33]. The nature of the pore is controlled by several processing variables such as green density, sintering temperature and time, alloying additions, and particle size of the initial powders [34]. In particular, the fraction, size, distribution, and morphology of the residual pores have a profound impact on the mechanical properties [35-37].

Regardless characterized by these residual pores, the compacts are considerably utilized as structural parts, and the demand has been expanded favorably in wide variety of engineering fields. As a result, higher density and high mechanical properties have been required to the sintered structural parts. As one of the solution, MIM technique is found to be the best candidate as a manufacturing process for meeting the above requirements, because MIM process offers near full dense and net shaping of complicated components with a relatively low processing cost [35].

When mechanical properties of the steel compact is considered, residual pores are not the only factor, the microstructural morphology is equally crucial, especially in high density compacts. Some alloy compact provides perfect homogenous nature, while the others are characterized by heterogeneous microstructure. Usually, when dealing with high-performance steel compacts, the nature of the microstructure is established on

multiphase and heterogeneous. Especially for superhigh strengthened Fe-Ni steel compacts, the microstructure is characterized with complex variations of Ni concentration [2-5]. And this is a subject of interests to be explored on how this heterogeneity nature affects the mechanical properties of the superhigh strengthened Fe-Ni steel compact.

1.1.4 Metal Injection Molding Process

Metal injection molding (MIM) offers several advantages over other production technologies. The MIM technology has progressed substantially over the past 25 years and the maturity of the technology is demonstrated by the growing number of components, alloys, size, and shape complexity. Complex-shaped parts can be simply manufactured by MIM process without or with very little secondary finishing. Also, undercuts in the parts, which are impossible with conventional sintering processes, can be realized with the MIM process. The surface of MIM parts is far superior to that of precision cast parts. Thereby, finishing and polishing costs can be eliminated or reduced. MIM parts usually do not have to be mechanically refinished, the harder the machined material is, the more advantageous the MIM process is. Summary of advantages offered by the MIM process is shown in Fig. 1.2 [29,37].

Although relatively expensive equipment are needed for MIM, the process is competitive, above all, in the fields where greater quantities of complicated products are required. Smaller products are usually manufactured by MIM process because tolerance deviations increase with the size of the product. The greatest advantage of the MIM process is that all sintering-suitable (sinterable) materials can be processed for complicated shapes.
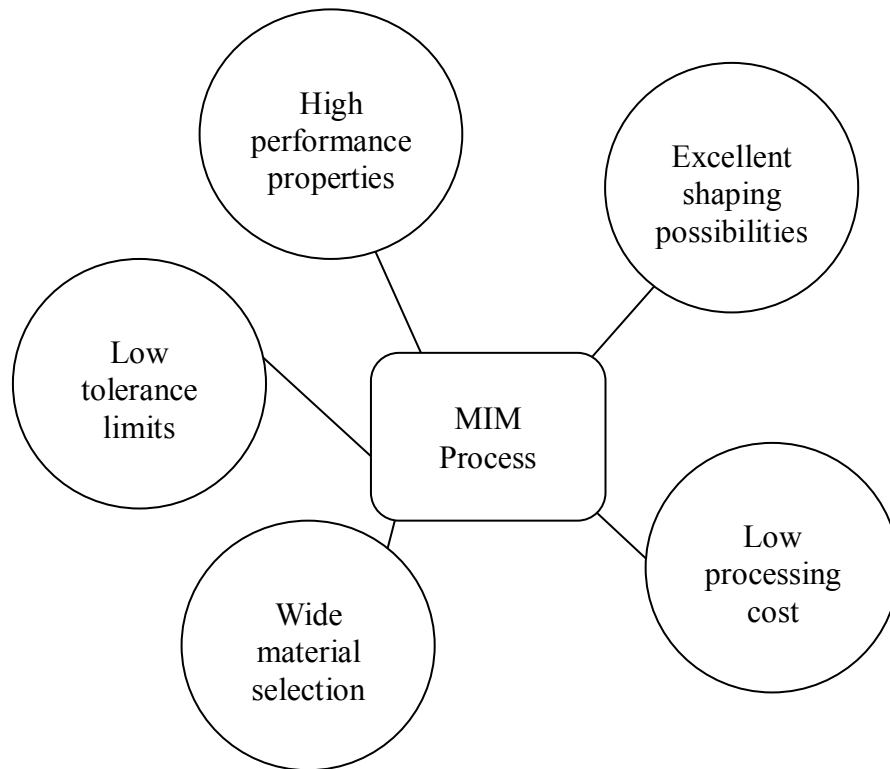
Fig. 1.2 The advantages of MIM process.

Another good point about MIM process, the feedstock material can be recycled nearly 100 %. This will give high benefit in cost reduction especially for the expensive materials. The total cost of mold, and equipment for debinding and sintering processes can be reduced by increasing the amount of production. In other words, the mass production is suitable for low cost of MIM process. The summary is that, to produce complex components at low cost, MIM process is expected to be one of suitable processes. Furthermore, it is possible to treat the components thermally or mechanically in order to achieve higher mechanical properties, narrower tolerances and lower surface roughness.

To know when in the process the heterogeneity occurred in the compact, flow of the MIM process should be explained here. In this study, promotion of heterogeneity structure into the compact begins at a very first instance during fabrication process. Two different elemental powders were prepared; Fine carbonyl Fe, and ultra-high pressure water-atomized Ni. These elemental powders were gently blended to form a balance dispersal of Fe and Ni particles in the powder mixture. It also has been reported that the heterogeneous microstructure of alloy containing Ni is easily attained. During sintering step, when Ni diffuses into Fe matrix, the carbon tends to repel the Ni, since Ni increases the chemical potential of carbon [38].

The flow of the MIM process is illustrated in Fig. 1.3. The process of metal injection molding is very similar to that of polymers [25,28-29]. The size of the powder particles ranges between 1 µm and a few of 100 µm. The most appropriate size of an individual particle for the process of MIM is smaller than 30 µm, and the average size of a particle is approximately 6 to 7 µm. The powder particles can be of various shapes, although the desired shape is a round one. As a result, it is possible to overcome certain anisotropic characteristics of a product while shrinking.

Molding is done by a conventional injection molding machine. The mold is designed similar to that for polymer but with consideration of shrinkage during subsequent debinding and sintering process. The parts are removed from the mold. At this point, the part known as "green" parts.

Before sintering, binder has to be removed. The binder is removed by heating, chemical extraction, or catalytic reaction. The debound part is called "brown". The binder removal process is called the debinding process.

The brown parts then subjected to sintering process. The purpose of sintering is to densify the powder and to remove most of the void space. The final density of the sintered part reaches from 94-99 % of the theoretical density. Ability to acquire high density compact which is comparable to the wrought alloys, is a crucial factor that contribute to the excellent mechanical properties offered by the compact.
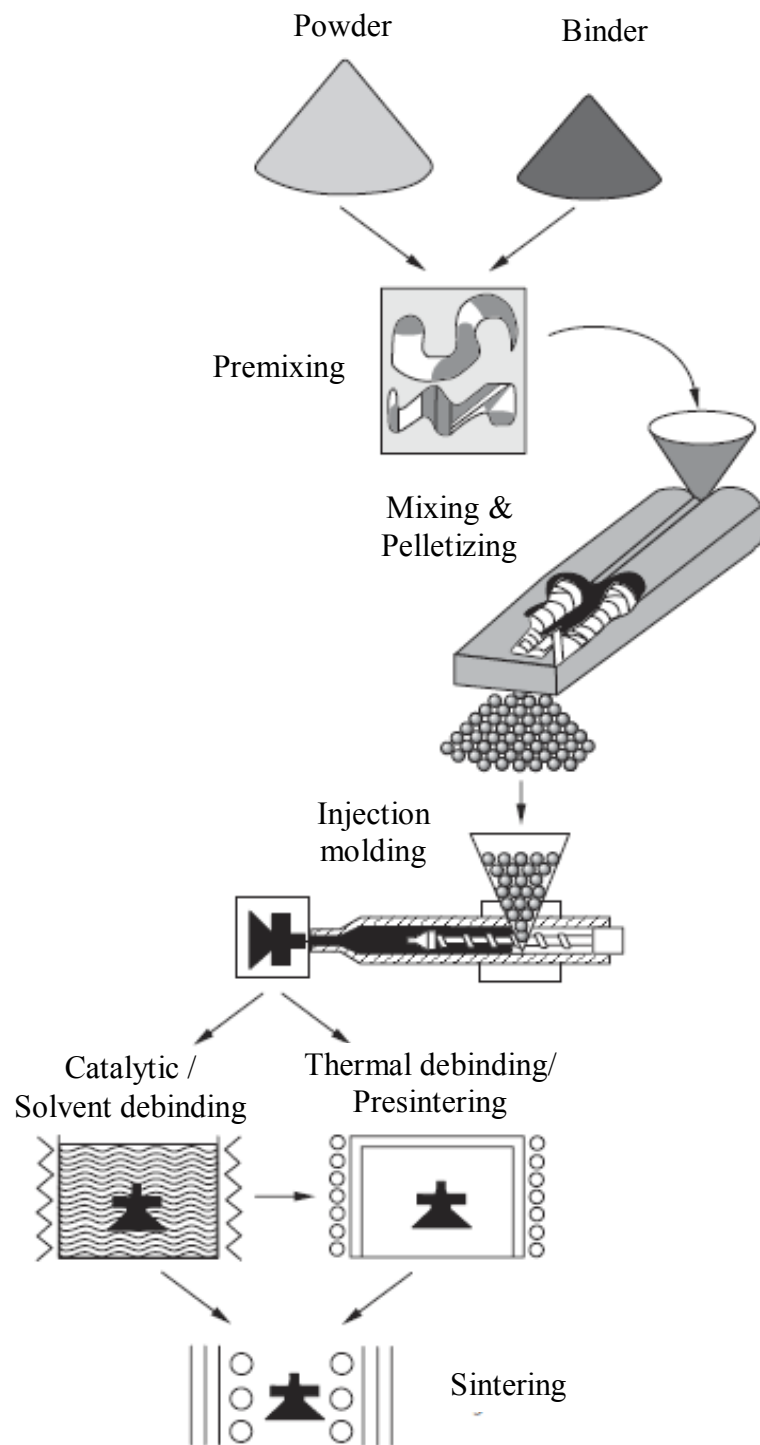
Fig. 1.3 Schematic diagram of MIM process [28,37].

1.2 OBJECTIVE OF STUDY

The work presented in this thesis is a first steps in understanding the complex microstructural morphology of the superhigh strengthened MIM Fe-Ni steel compacts at micro level. The experimental works have been extended numerically for more comprehensive studies of the matter. The data gathered here will serve as the foundation for the continuing design and development through understanding and careful control of microstructure and its effect on the properties of high-performance alloy compacts due to their heterogeneous and multiphase nature.

Firstly, the work began by systematically examination of the effect of residual pores on the tensile behavior of high strengthened steel compact experimentally, before continued by numerical simulation for verification. The 440C steel compact was selected as a model material. Although the compact was comprised by many residual pores, the compact offered high strength with homogenous microstructure. Three different compact densities were examined. Two-dimensional (2D) pore-based numerical models were then utilized for simulation of the compacts with various natures of pores cluster in order to efficiently gauge the effect of pores to their mechanical properties performance. The simulated mechanical properties results were then compared to experimentally obtained data.

The primary focus of this study is to clarify and to optimize the relationship between mechanical properties and the nature of heterogeneous microstructure for superhigh strengthened Fe-Ni steel compact through varying particle size of the Ni powders, Ni contents, and sintering conditions (temperature and time). In this study, the heterogeneity structure is mainly referred to the various concentration of Ni content throughout the compact matrix. There are two microstructural regions have been identified that play important roles in controlling mechanical properties; the higher Ni region, and the surrounded matrix (lower Ni region). These regions are the fundamental elements of complex Ni network of superhigh strengthened Fe-Ni steel compact. From crystalline structure point of view, the higher Ni is the region of Ni rich phase while the

lower Ni region structured by the tempered martensite [1]. Thus, a thorough understanding about the nature of this complex heterogeneous Ni structure is needed before further adventures into reinforcement phase of the superhigh strengthened Fe-Ni steel compact.

Further efforts through FEM modeling to characterized unique connections between variations of Ni content to their mechanical properties have been carried out. This has been done by creating micromechanical models based on the microstructural data available experimentally. Modeling by the FEM was divided into three different parts; geometry, boundary conditions, and constitutive material properties.

1.3 OUTLINE

A general introduction is given in Chapter 1 together with its comprehensive background information about superhigh strengthened Fe-Ni steel compact, microstructural simulation, steel compact, and injection molding process. The chapter also clarified objectives of the study. Then, Chapter 2 describes comprehensive studies about the effect of residual pores on the mechanical properties of the high strength steel compacts through experimental followed by FEM analysis. After the effect of pores on the mechanical properties is concluded, an experimentation of superhigh strengthened Fe-Ni steel compacts continued in Chapter 3. All data obtained from experimental works are appropriately presented and discussed. In Chapter 4, FEM simulation of superhigh strengthened Fe-Ni steel compact is performed. The 2D microstructure-based model is developed based on actual heterogeneous microstructure that of experimentally obtained from Chapter 3. In Chapter 5, all conducted research works are thoroughly concluded. The chapter also gives clear directions of possible future works about current study.

1.4 REFERENCES

1)   H. Miura, M. Matsuda : "Superhigh Strength Metal Injection Molded Low Alloy Steels by In-Process Microstructural Control", Material Transactions, 43 (2002) 343-347.

2)   H. Miura, M. Matsuda : "Ultrahigh strengthening sintered low alloy steels by advanced powder processing-MIM", J. Advanced Science, 13 (2001) 348-352.

3)   M. Matsuda, H. Miura : "Mechanical Properties of Injection Molded Fe-6%Ni-0.4%C Steels with Varying Mo Contents of 0.5 to 2%", Metals and Materials International, 9 (2003) 537-542.

4)   H. Miura : "High Performance Ferrous MIM Components Through Carbon and Microstructural Control" Materials and Manufacturing Processes, 12 (1997) 641-660.

5)   H. Miura, S. Mitomi, S. Ando, T. Honda : "Effect of homogeneous and heterogeneous structure on the properties of sintered alloy steels by MIM", J. Jpn. Soc. Powder Powder Metallurgy, 42 (1995) 378-382.

6)   H. Zhang, R.M. German : "Homogenization and Microstructure Effects on the Properties of Injection Molded Fe-2Ni Steel", Metallurgical and materials Transactions A, 23 (1992), 377-382.

7)   H. Zhang, R.M. German : "Sintering MIM Fe-Ni alloys", Int J. of Powder Metallurgy, 38 (2002) 51-61.

8)   H. Zhang, R.M. German : "Homogeneity and properties of injection moulded Fe-Ni alloys", Metal Powder Report, 56 (2001) 18–22.

9)   K.-S. Hwang, C. Hsu, L.-H. Cheng, P.-H. Chen : "Ultrahigh-strength sinter-hardening MIM alloy steels", Int J. of Powder Metallurgy, 48 (2012) 35-43.

10)   N. Chawla, KK. Chawla : "Metal matrix composites", New York, Springer, (2006) 137.

11)   Z. Hashin, S. Shtrikman : "A variational approach to the theory of the elastic behavior of multiphase materials", J. Mech Phys Solids, 11 (1963)127-40.

12)   JC. Halpin, SW. Tsai : "Effect of environmental factors on composite materials", Air Force Material Lab, TR 67 (1967) 423.

13)   T. Mura : "Micromechanics of defects in solids", 2nd ed. The Hague: Martinus Nijhoff; (1987).

14)   T. Mori, K. Tanaka : Average stress in matrix and average elastic energy of materials with misfitting inclusions", Acta Metall. 21 (1973) 571–574.

15)   J. Llorca, A. Needleman, S. Suresh : "An analysis of the effects of matrix void growth on deformation and ductility in metal-ceramic composites", Acta Metall. Mater., 39 (1991) 2317–35.

16)   J.R. Brockenbrough, S. Suresh, H.A. Wienecke : "Deformation of metal-matrix composites with continuous fibers: Geometrical effects of fiber distribution and shape", Acta Metall. Mater., 5 (1991) 735-52.

17)   Y.L. Shen, M. Finot, A. Needleman, S. Suresh : "Effective elastic response of two-phase composites", Acta Metall. Mater., 42 (1994) 77–97.

18)   J. Segurado, C. Gonzalez , J. Llorca : "A numerical investigation of the effect of particle clustering on the mechanical properties of composites", Acta Mater., 51 (2003) 2355–69.

19)   J. Boselli, PD. Pitcher, PJ. Gregson, I. Sinclair : "Numerical modeling of particle distribution effects on fatigue in $Al - SiC_p$ composites", Mater. Sci. Eng. A300 (2001) 113-24.

20)   M. Li, S. Ghosh, T.N. Rouns, H. Weiland, O. Richmond and W. Hunt : "Serial sectioning method in the construction of 3-D microstructures for particle reinforced MMCs", Materials Characterization, 41 (1998) 81-95.

21)   M. Li, S. Ghosh and O. Richmond : "An experimental-computational approach to the investigation of damage evolution in discontinuously reinforced aluminum matrix composite", Acta Materialia, 47(12) (1999)3515-32.

22)   S. Ghosh and S. Moorthy : "Three dimensional Voronoi cell finite element model for modeling microstructures with ellipsoidal heterogeneities", Computational Mechanics, 34 (6) (2004) 510-31.

23)   W. Han, A. Eckschlager, H.J. Böhm : "The effects of three-dimensional multi-particle arrangements on the mechanical behavior and damage initiation of particle-reinforced MMCs", Compos. Sci. Technol., 61 (2001) 1581–1590.

24)   A. Eckschlager, W. Han, H.J. Böhm : "A unit cell model for brittle fracture of particles embedded in a ductile matrix", Compos. Sci. Technol., 25 (2002) 85–91.

25)   R. A. Lula : "Stainless Steel", American Society for Metals, Metals Park, OH (1986) 37-39.

26)   P. K. Samal, J.C. Valko, J.D. Pannell : "Processing and Properties of P/M 440C Stainless Steel", Advances in Powder Metallurgy & Particulate Materials–2009, Part 7 (2009) 112-121.

27)   E. Klar, P. K. Samal : "Powder Metallurgy Stainless Steels: Processing, Microstructures, and Properties", ASM International (2007) 20.

28)   R.M. German, A. Bose : "Injection Molding of Metals and Ceramics", Metal Powder Industries Federation, Princeton, NJ (1997) 3.

29)   R.M. German : "Powder Metallurgy of iron and steel", Wiley-interscience (1990) 73-78.

30)   K. S. Hwang, Y. M. Hsieh : "Comparative Study of Pore Structure Evolution During Solvent and Thermal Debinding of Powder Injection Molded Parts", Metallurgical and Materials Transactions A 27A (1996) 245-253.

31)   R.M. German : "Sintering Theory and Practice", John Wiley & Sons (1996) 421-444.

32)   D. Li, H. Hou, L. Liang, K. Lee : "Powder Injection Molding 440C Stainless Steel", Int J Adv Manuf Technol., 49 (2010) 105-110.

33)   D. Peckner, I.M. Bernstein : "Handbook of Stainless Steels", McGraw-Hill, (1977) 6-19.

34)   A. Salak : "Ferrous Powder Metallurgy", Cambridge International Science Publishing, Cambridge (1997).

35)   A. Hadrboletz, B. Weiss: "Fatigue Behavior of Iron Based Sintered Material: A Review", International Mater., 42 (1997) 1-44.

36)   N. Chawla, S. Polasik, K.S. Narasimhan, M. Koopman, K.K. Chawla : "Fatigue Behavior of Binder-Treated P/M Steels", Int. J. Powder Metall., 37 (2001) 49-57.

37)   R.M. German : "Powder Injection Molding", MPIF, Princeton, NJ (1990) 3-17.

38)   A. L. Sozinov, V. G. Gavrilijuk : "Estimation of Interaction Energies Me-(C, N) in F. C. C. Iron-Based Alloys Using Thermo-Calc Thermodynamic Database", Scripta Mater., vol. 41, issue 6 (1999) 679-683.

CHAPTER 2

Effect of Pores on the Mechanical Properties of High Strengthening Steel Compacts

2.1 INTRODUCTION

Though the general effects of pores on the tensile behavior of MIM compacts have been reported [1-5], a comprehensive and quantitative understanding of the effect of pores on the mechanical properties of MIM compacts is still not enough. Although the steel compact demonstrated high strength characteristics with homogeneous microstructure, many residual pores are also found throughout the matrix. Since the pores decrease mechanical properties, this is a common challenge when dealing with any alloy steel fabricated by P/M process. In this chapter, the effect of pores on the tensile behavior of a high strengthened steel is systematically examined using experimental and numerical techniques. Finite element method (FEM) was used to simulate the microstructural effect. Similar methodology will be also utilized to evaluate the heterogeneous microstructure of superhigh strengthened Fe-Ni steel compact in chapter 4.

The 440C stainless steel was employed as an example material to evaluate the effect of pores. It is a high carbon martensitic stainless steel with moderate corrosion resistance, high strength, excellent hardness and wear resistance. Due to these excellent properties, the steel has been used for many applications, such as ball bearings and races, gage blocks, molds and dies, knives and measuring instruments. However, when high strength 440C steel compact is considered over wrought alloy steel, many residual pores are typically characterized usually after sintering, which quite detrimental to their mechanical properties [6-7].

In this chapter, the main factor investigated by a series of experiments was on variability of the powder loading of the 440C alloy steel feedstock. As a high performance process, MIM has very high demands on compact with high sintered density. In this respect, the powder loading of a feedstock plays a key role. It has to be as high as possible in order to obtain higher densification during sintering. On the other hand, if it is higher than critical powder loading, this may result in lower sintered density due to increase in resistance between powder particle during injection molding

and may cause process instability. The importance of the powder loading for obtaining good sintered density or less residual pores has been widely discussed in the literature [8-9].

Quantitative analysis on the microstructure of the high strength steel compact was then performed in order to determine the pore size distribution and the pore shape. Finally, pore microstructure-based numerical models were successfully developed to simulate tensile strength and elongation behaviors, before compared with experimentally obtained data.

2.2 EXPERIMENTAL METHOD

2.2.1 Powder Characteristic

An ultra-high pressure water-atomized 440C stainless steel powder was supplied by Mitsubishi Steel Mfg. Co. Ltd., Japan (MHT440C). The mean particle size was in the range of 9 to 12 μm (D_{50}=9.64 μm). As shown in Fig. 2.1, the powder shapes were dominated by irregular which will provide an excellent inter-locking effect between particles in the compact [10]. However, it also has a major influence on the apparent density, flow properties, green strength, and compressibility of the powder; it also affects sintered properties, including dimensional change and mechanical properties. The irregularity of the shapes causes more contact points between particles during molding.

Therefore, higher compacting pressure was required to achieve proper green compact density, which is related to mechanical properties after sintering [11-12]. More detailed powder characteristics are given in Table 2.1.
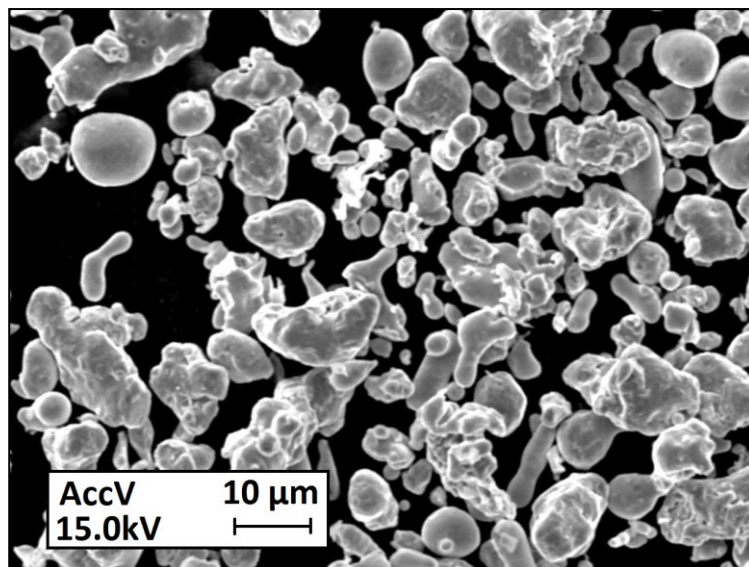
Fig. 2.1 SEM photomicrograph of 440C stainless steel particles.

Table 2.1 Properties of 440C stainless steel powder in the present study.

| Powder Characteristics	
Chemical Composition (mass%)	16.65Cr, 1.07C, 0.99Si, 0.3Mn, 0.019S, 0.015P, 0.37O, Bal. Fe
Average Particle Size	D_{50}=9.64 μm
Production Technique	Water-atomization
Average Shape	Rounded, ligament
Pycnometric Density	7.60 g/cm^3
Supplier	Mitsubishi Steel Mfg. Co. Ltd., Japan

2.2.2 Binder Characteristic

A wax-polymer binder system which is commonly used in MIM was selected for this study. The system consists of four binder components; paraffin wax (PW), atactic polypropylene (APP), carnauba wax (CW), and stearic acid (SA). The components can be divided principally into two groups based on their molecular weight;

soluble and insoluble [13-14]. The soluble binder components which typically have lower molecular weight consists of PW and SA. Whereas, APP and CW are binder components with higher molecular weight. Detailed characteristics of these binder components and composition are shown in Table 2.2. The removal of polymeric binders, or debinding, is a very critical step in the MIM process because of defects during the process such as cracking, blistering, and distortion [15-17].

Thermogravimetric analysis (SSC5200, Seiko) of the binder components and the feedstock under N_2 atmosphere was carried out to determine thermal debinding schedules. In normal circumstances, each binder component will be tracking a single sigmoidal path for their TGA decomposition curves. Apparently, Fig. 2.2 shows that within the temperature range of 190 and 480 ºC, all of binder components were effectively decomposed. Figure 2.3 shows the rate of decomposition for each binder component, mixture of the binder components, and binder in feedstock. Additionally, two or more sigmoidal paths were found on the curves for a mixture of multi-component binders due to difference in their molecular weights, bonding groups, and decomposition paths of various polymer components as shown in Fig. 2.3.

Table 2.2 Characteristic of binder system for 440C stainless steel.

Binder Component	PW	APP	CW	SA
Ratio (mass%)	69	20	10	1
Melting Point (ºC)	56 to 58	> 95	80 to 86	67 to 69
Density (g/cm³)	0.895	0.854	0.995	0.941
Supplier	Sigma-Aldrich Japan	Tarui Chemical Industry Co., Ltd, Japan	Sigma-Aldrich Japan	Sigma-Aldrich Japan
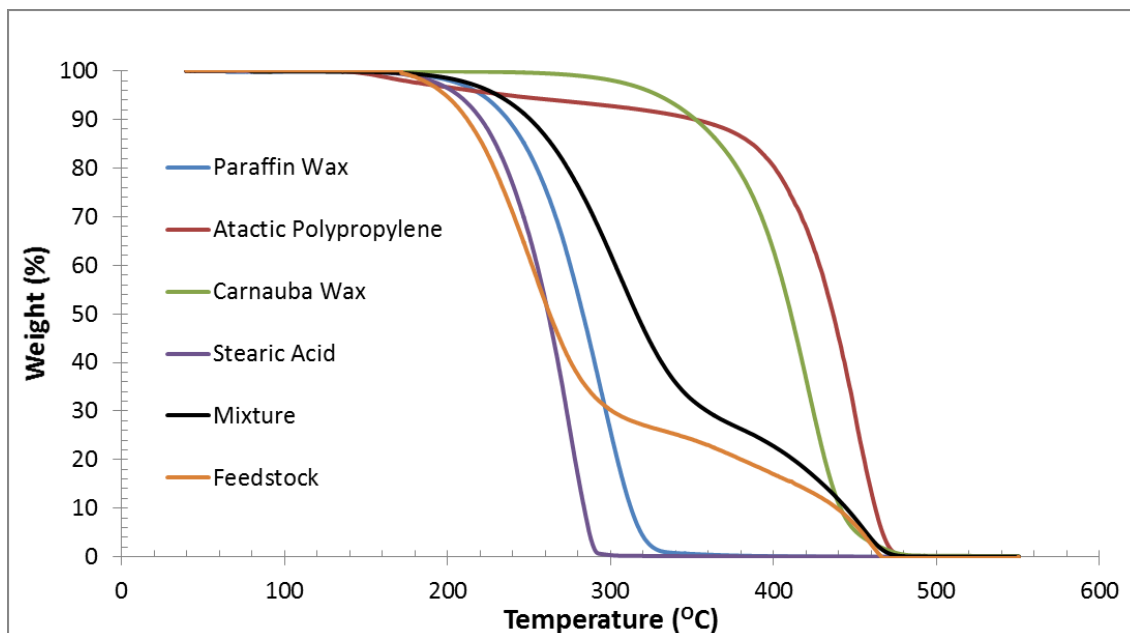
Fig. 2.2 Weight decomposition for each binder component, mixture, and feedstock at heating rate of 10 °C/min
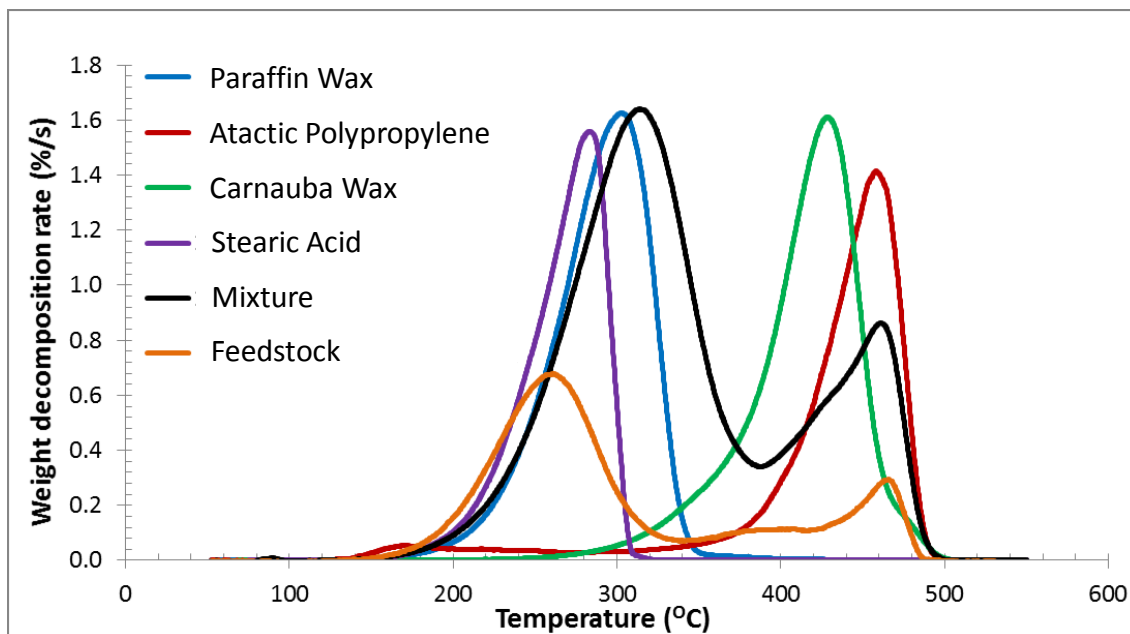
Fig. 2.3 Weight decomposition rate for each binder component, mixture, and feedstock at heating rate of 10 °C/min.
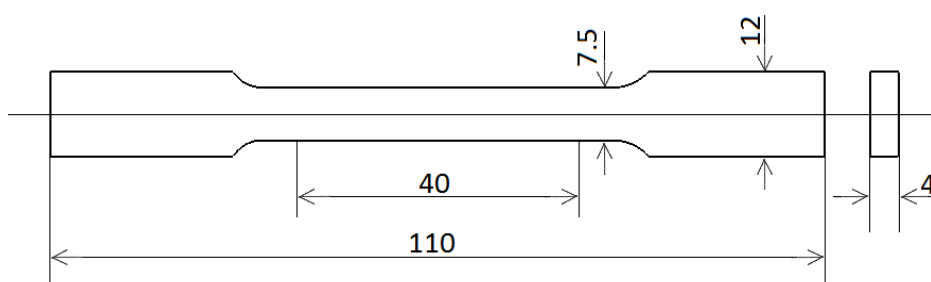
2.2.3 The Compact

Compact used in this work was a flat-bar tensile shape. Detailed dimension of flat-bar tensile compact utilized in this study are as specified in Fig. 2.4.

2.2.4 Experimental Procedure

Three levels of powder loading were prepared for the present study. Powder loading of 60, 63, and 64 % by volume fraction was mixed with the binder system to form a feedstock. Binder material was consisted of 69 mass% paraffin wax (PW), 20 mass% atactic polypropylene (APP), 10 mass% carnauba wax (CW), and 1 mass% stearic acid (SA) as shown in Table 2.2. The powder and the binder materials were kneaded by Z-blade mixer (5DMV-01-rr, Dalton) at 150 ℃ for 1.5 hours to ensure homogenous mixture prior to pelletizing to the formation of homogenized feedstock. The compact as shown in Fig. 2.4 was molded by an injection molding machine (JC50SA II, Japan Steel Works Ltd).

Solvent debinding method was employed for the first step of binder removal in this work. The green compact was keeping within 54 to 56 ℃ in a solvent container of vaporized heptane for 4 hours followed by thermally debinding in pure hydrogen (for hydrogen sintering) or in argon (for partial vacuum sintering) atmosphere with heating rate 2 ℃/min up to debinding temperature at 600 ℃ for 1 hour. The debound compact was then sintered in the same furnaces at three different temperatures of 1240, 1250 and 1260 ℃ for 30 minutes. Hydrogen sintering was carried out in the electrical furnace (TSH-1060, Siliconit) and vacuum sintering was in vacuum furnace (VHLgr20/20/20, Shimadzu Mectem Inc.) at 10^{-1} Pa.

**Fig. 2.4 Dimensions of flat-bar tensile compact.**

The sintered compact was then heat treated by cryogenic quenching before brought into testing. The cryogenic quenching was carried out in a liquid nitrogen bath (-196 ℃). The sintered compact was reheating in pure hydrogen atmosphere at 1000 ℃ for 30 minutes, then oil-quenching to room temperature. Immediately the compact was immersed into the liquid nitrogen and remains for 30 minutes, and then tempered for 2 hours at 180 ℃ in argon atmosphere.

Archimedes technique of water immersion was employed for density measurement of all sintered compacts. The carbon and oxygen contents in both sintered and heat treated compacts were determined by carbon combustion analyzer (EMIA-110, HORIBA) and nitrogen/oxygen determinator (TC-500SP, LECO), respectively. Hardness was measured by micro Vickers-hardness tester. The heat treated compacts were finally subjected to tensile testing. Five compacts were pulled into failure for each condition and the ultimate tensile strength and elongation were determined by their average.

2.3 RESULTS AND DISCUSSION

### 2.3.1 The Effect of Powder Loading on the Mechanical Properties of High Strength 440C Steel Compact

Pore structure of the compacts with three different powder loadings are shown in Fig. 2.5. Higher powder loading simply decreased the porosity of the compact. The sintered density at powder loading 64 vol% (PL-64 %) (95.3 %) has not been increased as compared to the compact at powder loading 63 vol% (PL-63 %) (95.5 %). This indicates that PL-63 % was a critical powder loading at which the binder composition was just sufficient enough to completely fill the inter-particulate spaces for 440C steel compact in this study. Figure 2.6 shows the porosity fraction at different sintering temperature for PL-60 %, PL-63 %, and PL-64 %, where the compact with PL-63 % showed the least porosity or highest sintered density.

23
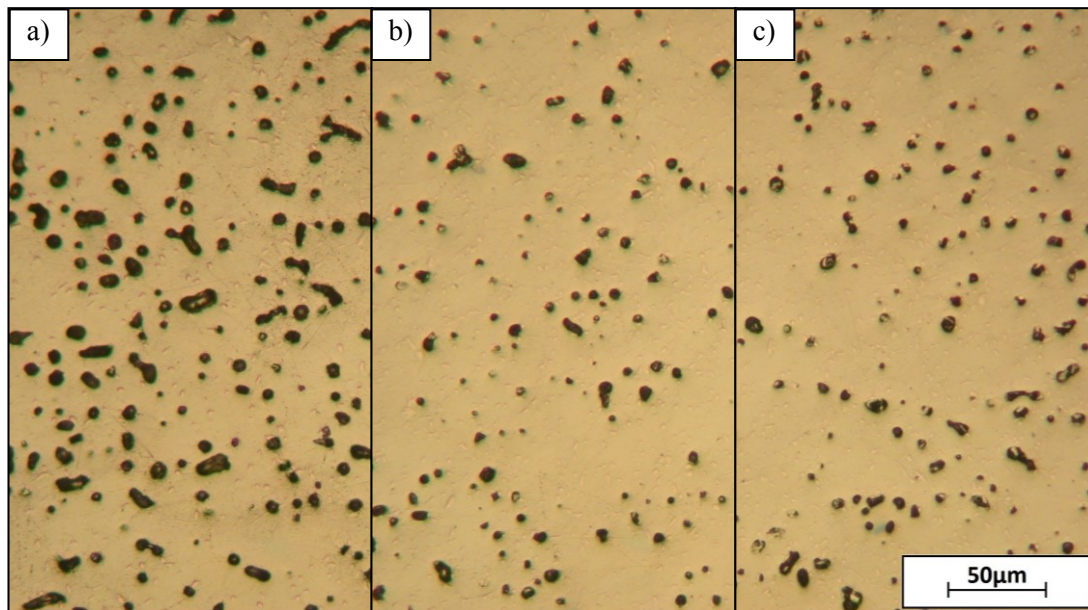
Fig. 2.5 Pore structure of partial vacuum sintered compacts at different powder

loading a) 60 vol%, b) 63 vol%, and c) 64 vol%.
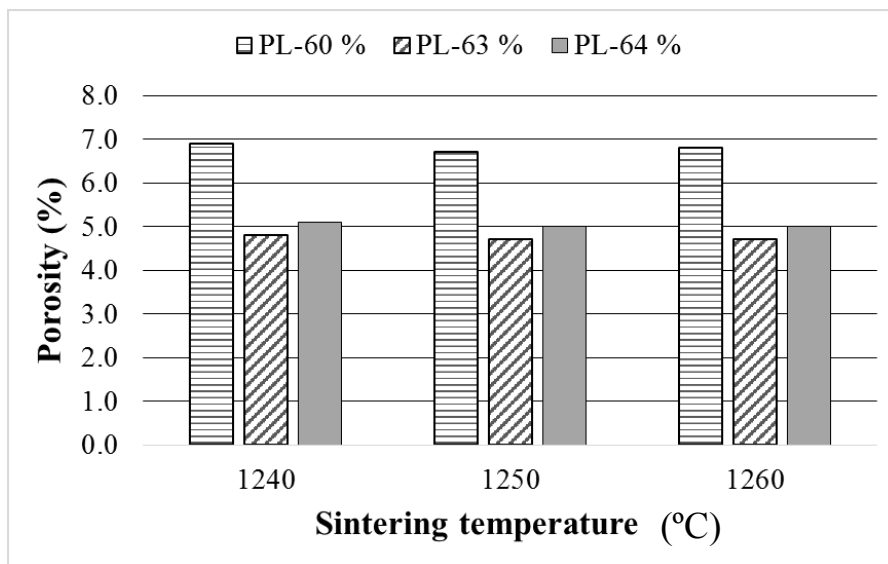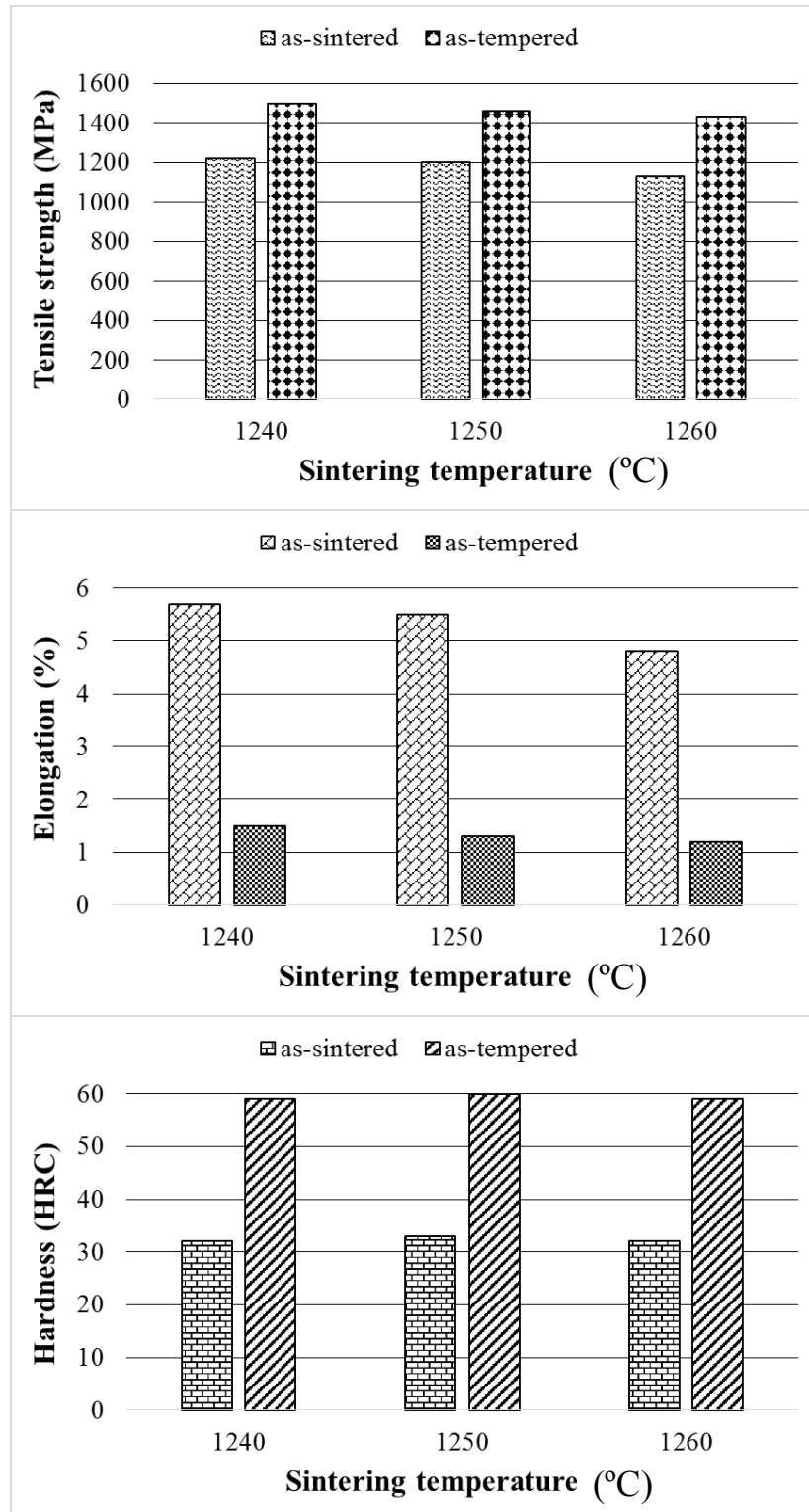

Fig. 2.6 The porosity of compact in partial vacuum atmosphere for PL-60 %,

PL-63 %, and PL-64 %.
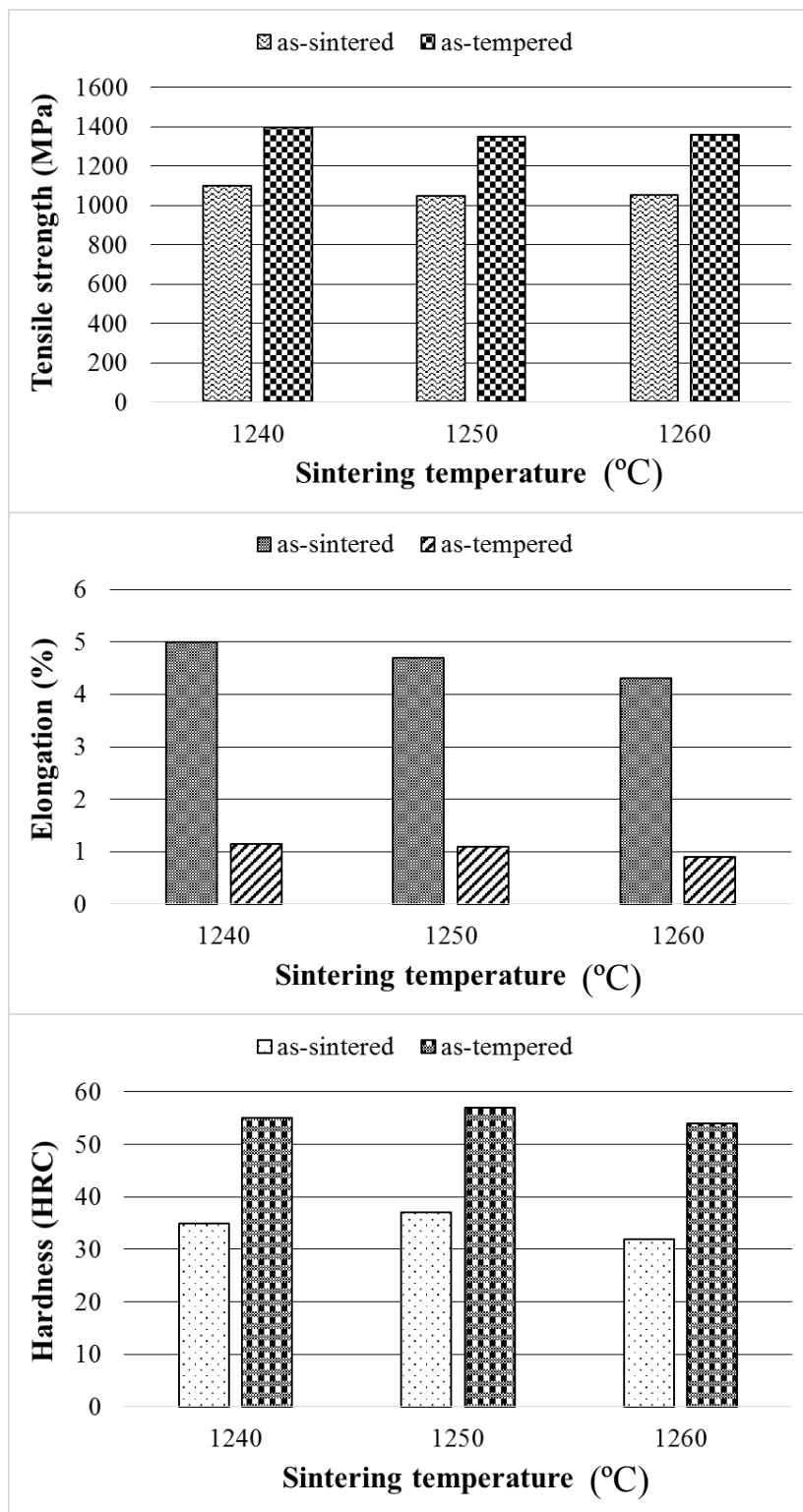
Fig. 2.7 Tensile strength, elongation, and hardenability at three sintering temperatures in partial vacuum for PL-60 % compact.

Fig. 2.8 Tensile strength, elongation, and hardenability at three sintering temperatures in partial vacuum atmosphere for PL-63 % compact.

The mechanical properties of PL-60 % and PL-63 % compacts at different sintering temperature are shown in Figs. 2.7, and 2.8, respectively. The PL-63 % compacts shows higher strength, elongation, and hardness as compared to the compacts with PL-60 %. The sintered density of PL-63 % compact was improved for about 2 % to 7.32 g/cm^3 from 7.14 g/cm^3. Whereas, the tensile strength and hardness have increased by 7 % to the highest strength of 1495 MPa and 11 % to 60 HRC, respectively, which are greater to those conventional P/M steels and similar or superior to wrought steels [18].

2.4 NUMERICAL SIMULATION

In this section, pore microstructure-based FEM model was constructed to simulate the progression of stress/strain by pores under tensile testing. The increase in ultimate tensile strength and improvement in ductility with reduced porosity can be explained by modeling the microstructure of each of the two steels (PL60 and PL63). The discussion from the previous section showed that the compact behavior was controlled by the microstructure nature of the compact, in particular the nature of the residual pores. Thus, in this study, two-dimensional (2D) microstructures based on actual pores distribution were employed for the finite element simulations. The optical microstructures in Fig. 2.9 were used as a basis for FEM analysis of uniaxial loading. More specifically, the models were developed exactly based on the defined region of interest (ROI) as shown in Fig. 2.9. Figure 2.10 shows the models with finite element meshes and boundary conditions. A finer mesh was employed around pore peripherals and a coarse mesh was implemented in the matrix-rich areas.
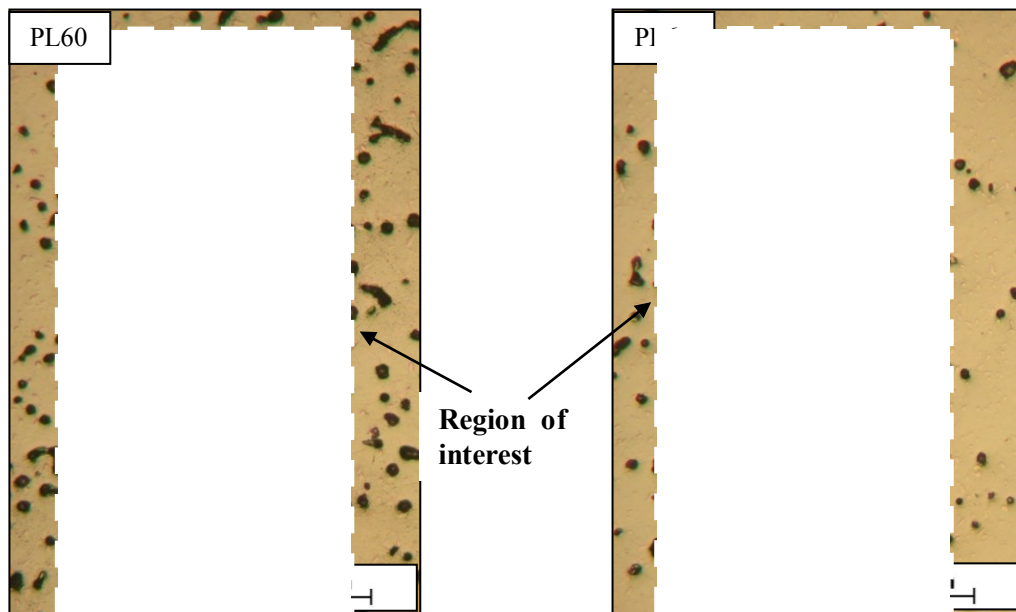
PL60

P[

Region of interest

Fig. 2.9 Optical microstructure of partial vacuum sintered compacts at different powder loading.

10 % strain

150 μm

PL60
7 % porosity
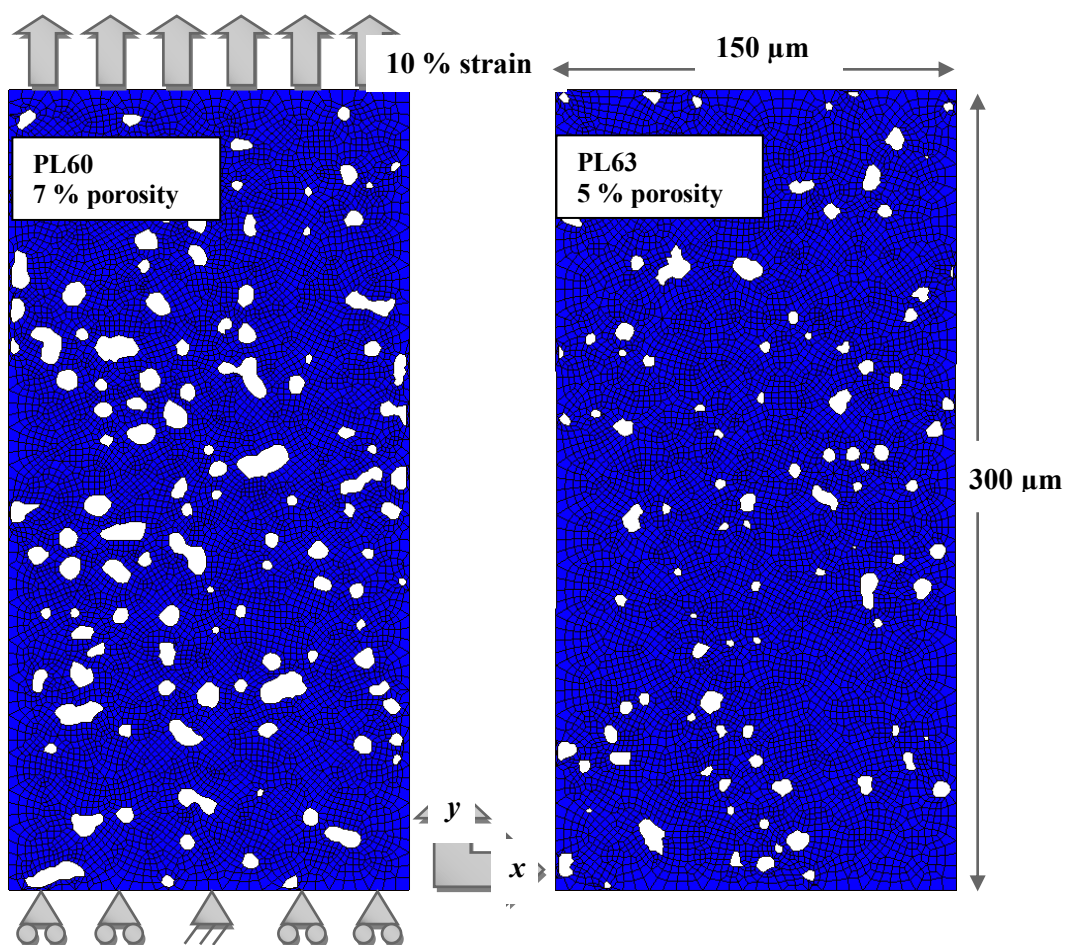
PL63
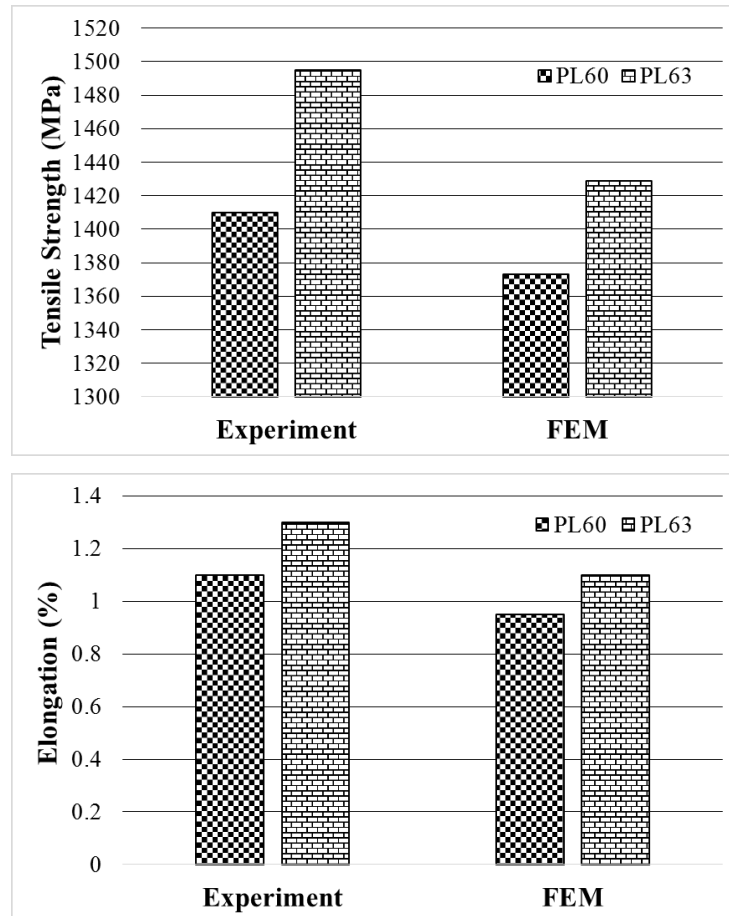5 % porosity

300 μm

y

x

Fig. 2.10 Finite element mesh and boundary conditions used for finite element analysis based on the real microstructure of 440C stainless steel compact.

The bottom edge was fixed in the vertical direction ($V_1 = 0$), while load was applied to the top edge vertically under control of displacement rate. An applied strain to the models was 10 %. Modified hexahedral meshes were employed in this simulation to conform the irregular nature of the microstructure. The Young's modulus and Possion's ratio were 200 GPa and 0.30, respectively. The Young's modulus obtained from experimentation data was utilized as an input into the models. And the Poisson's ratio was from a common available data for the alloy steels. Work hardening properties of the models were based on stress-strain curves obtained from experiment. In order to obtain accurate simulation results, the region of interest within actual microstructure used in the model should be large enough to provide adequate statistical representation.

The ultimate tensile strength and elongation data predicted by the models are shown in Fig. 2.11. Note that even a slight decrease in porosity (2 %) results in a significant decreases in strength of the compact, as was observed experimentally. The reason can be shown from the evolution of equivalent tensile stress in the microstructure, shown in Fig. 2.12. A large amount of stress localization took place in the regions between pores. In particular, networks of pores are quite effective in localization the stress in the ligaments between pores. Thus, a very small section of the microstructure is actually being plastically deformed, and a large portion of the compacts is undeformed. The results confirmed with experimental observations that pore causes deformation to be localized and inhomogeneous [19-21].

The stress intensification in the compact ligaments between pores likely serves as areas for crack initiation. Once the onset of crack initiation takes place, the large pores will be linked, and the local effective load bearing area of the compacts will decrease very quickly, resulting in fracture of the compact. An increase in porosity decreases the compact ligament fraction and spacing between pores, thus accelerating the intensification of stress in the compact matrix. Model also shows that plastic stress intensification begins at the tip of irregular pores in the microstructure. Vedula and Heckel [19] compared the damage mechanisms between round and angular pores in matrix with identical pore fractions and observed that highly localized slip bands

formed at the sharp tips of angular pores. This resulted in highly localized and inhomogeneous plastic deformation compared to the deformation around round pores which was much more homogeneous.

Fig. 2.11 Modeled data comparison of tensile strength and elongation by 2D FEM analysis. An apparent increase in strength and elongation is observed at 5 % porosity, commensurate with the experimental data.

The distribution of the pores is also important, since it has been shown that plasticity may initiate at pore clusters because of the higher localized stress intensity associated with these defects [22]. The stress distribution in the modeled microstructure for PL63 (Fig. 2.12 (b)) shows that when the pores are lesser, smaller, and more homogeneously distributed, the stress distribution is relatively more uniform and the deformation is more uniformly distributed throughout the matrix. Therefore, a slight

increase in density from 7.14 g/cm^3 to 7.32 g/cm^3 resulted in a significant increase in stress-to-failure, although the strength and elongation of the compact increased slightly. This may be attributed to narrower and more homogeneous distribution of pores in the PL63 versus PL60 compact, although the total amount of porosity in the latter compact was not significantly higher. Most of the stress localization takes place at the shortest distance between pores or pore clusters. In particular, most of the plastic deformation bands tend to be at an angle to the tensile direction, so the orientation of pores with respect to the loading axis may also play a significant role on plastic deformation.
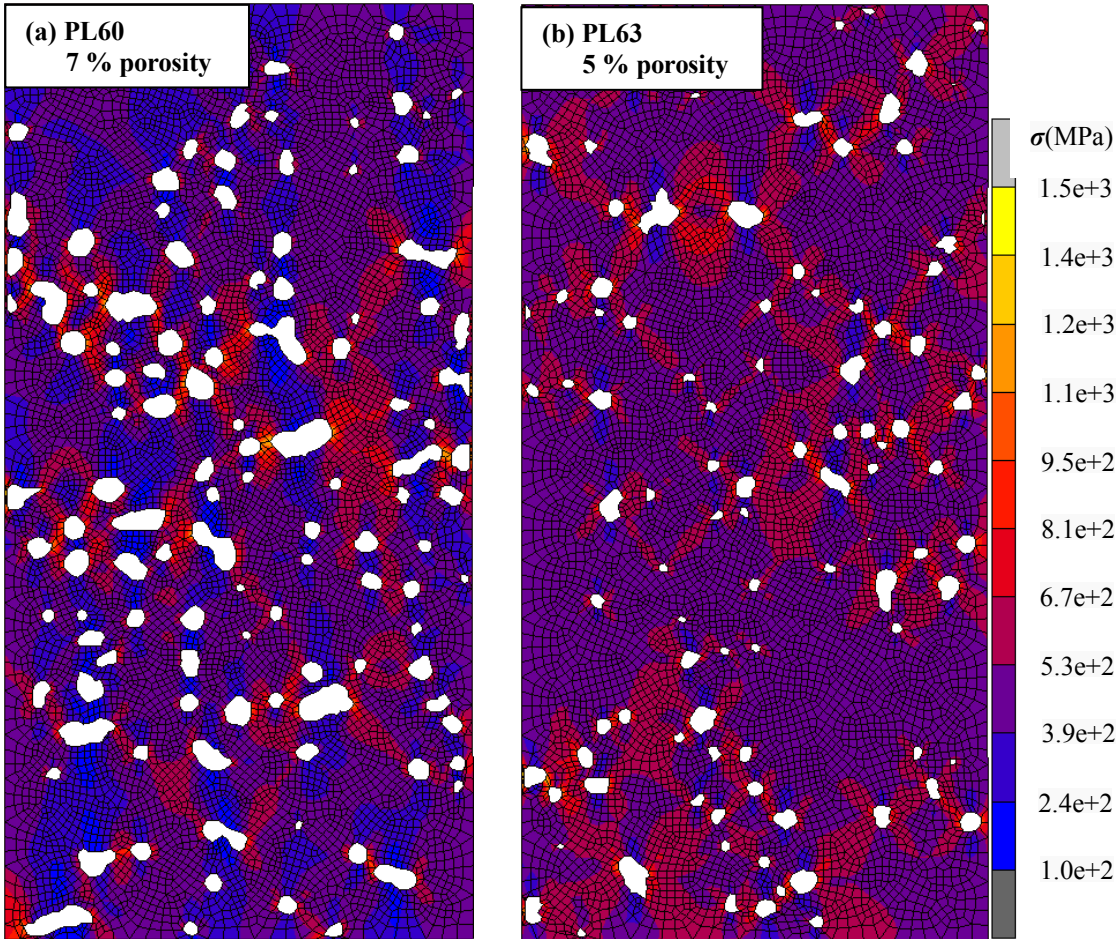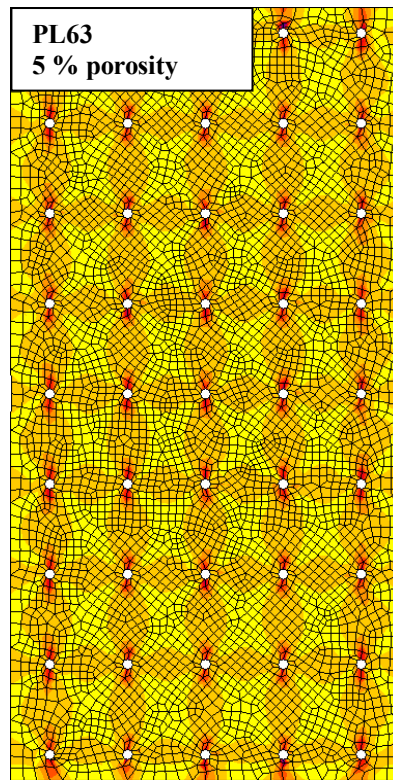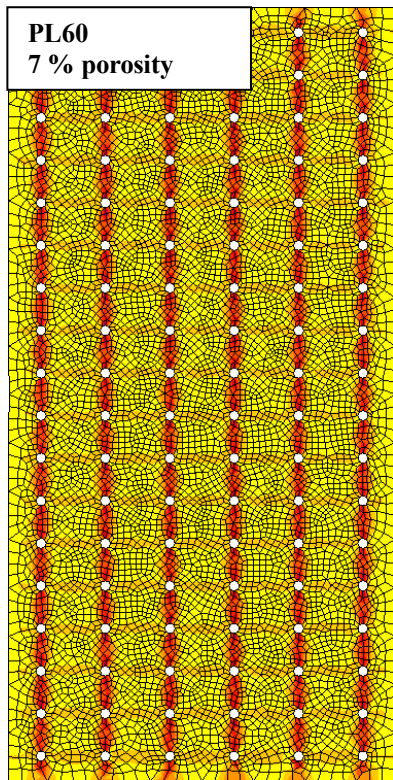

Fig. 2.12 Effective equivalent tensile stress contours in modeled microstructures: (a) PL60, and (b) PL63. Larger and interconnected pores cause strain intensification, while smaller, more homogeneously distributed pores contribute to more homogeneous deformation.

An equally important result of the model is that, even in the higher density compact, a large amount of stress intensification takes place at a single pore cluster in the microstructure (Fig. 2.12 (b)). Thus, even when the overall amount of porosity is relatively low (5 %), stress intensification may take place around the pore clusters. It follows by the homogeneity and distribution of the pore is as important as the fraction of porosity in controlling the evolution of plastic stress and strain, and thus the onset of crack initiation.

Furthermore, series of pattern models are also prepared; pattern 1, pattern 2, and pattern 3 with perfect round pores positioned in arrays as shown in Fig. 2.13. More detailed description about each pattern is summarized in Table 2.3. The pores fraction for both models PL60 and PL63 were remained identical as previous models; 7 and 5 %. Both models showed the stress distributed more evenly compared to PL60 and PL63 models throughout the matrix. Thus, it causes an elimination of stress localization between shortest distance between pores or pore clusters.

Table 2.3 Detail features for each model; Pattern 1, Pattern 2, and Pattern 3.

Model(Porosity)	Pattern 1	Pattern 2	Pattern 3
PL60 (7 %)	Pore Diameter: **2 µm** Pore Number: **108 unit**	Pore Diameter: **4 µm** Pore Number: **27 unit**	Pore Diameter: **6 µm** Pore Number: **12 unit**
PL63 (5 %)	Pore Diameter: **2 µm** Pore Number: **45 unit**	Pore Diameter: **4 µm** Pore Number: **11 unit**	Pore Diameter: **6 µm** Pore Number: **5 unit**

(a) Pattern 1
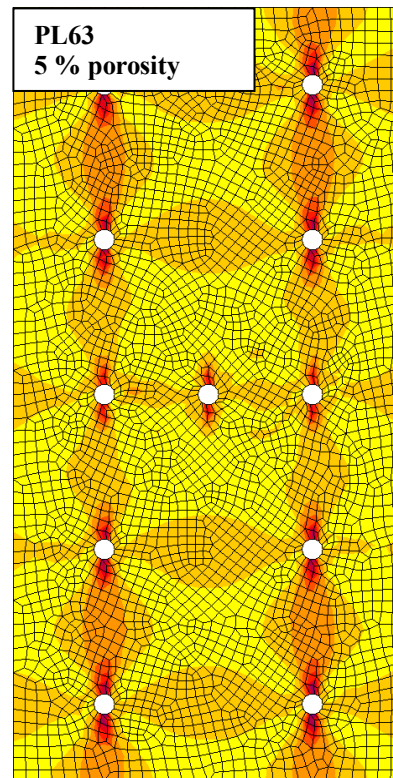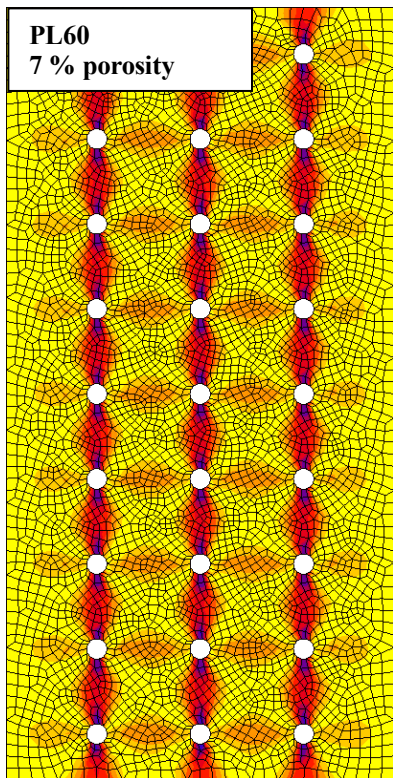
(b) Pattern 2
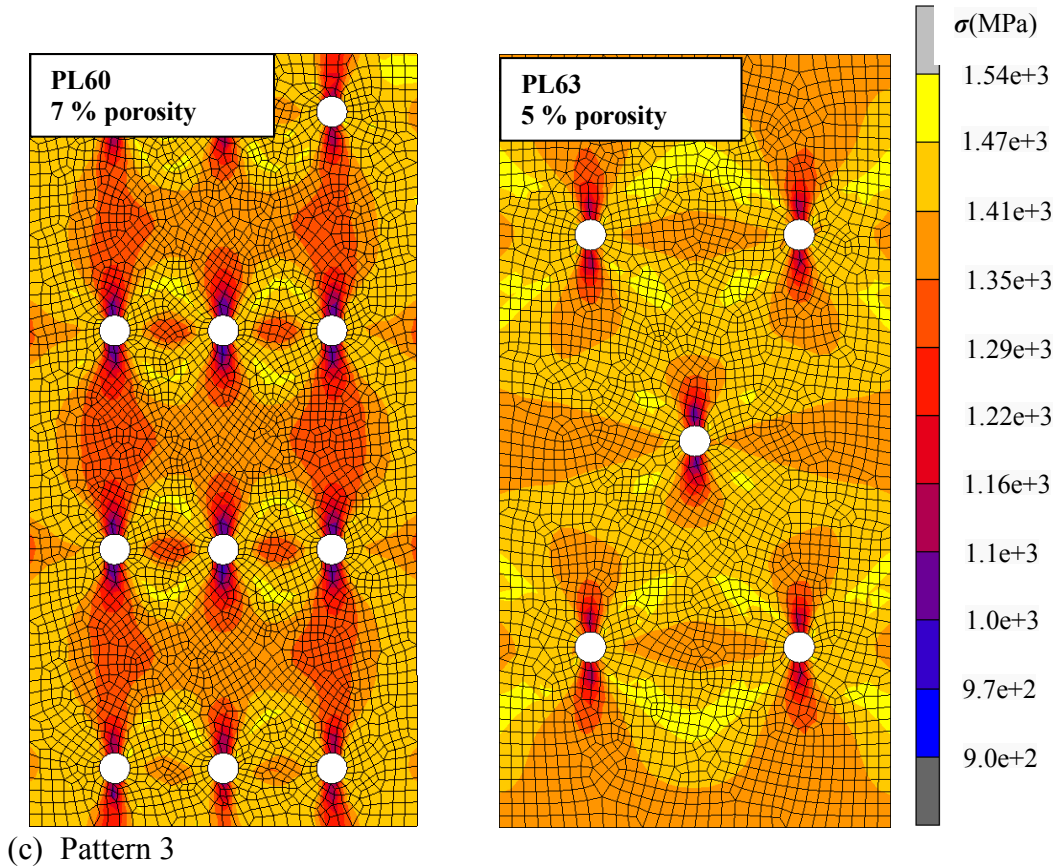
(c) Pattern 3

Fig. 2.13 Effective equivalent tensile stress contours in modeled microstructures: (a) Pattern 1, (b) Pattern 2, and (c) Pattern 3. Homogeneously distributed pores contribute to homogeneous stress deformation.

Figure 2.14 shows a comparison of simulated mechanical properties data of PL60 and PL63 compacts. Note that the simulated mechanical properties data of both compacts showed almost similar trends when the pores structures were reordered into pattern 1, 2, and 3 from the actual microstructure. At similar porosity level, reordering the pore pattern, variation of pore size and number seems to give minor influence on their mechanical properties as shown in Fig. 2.14.
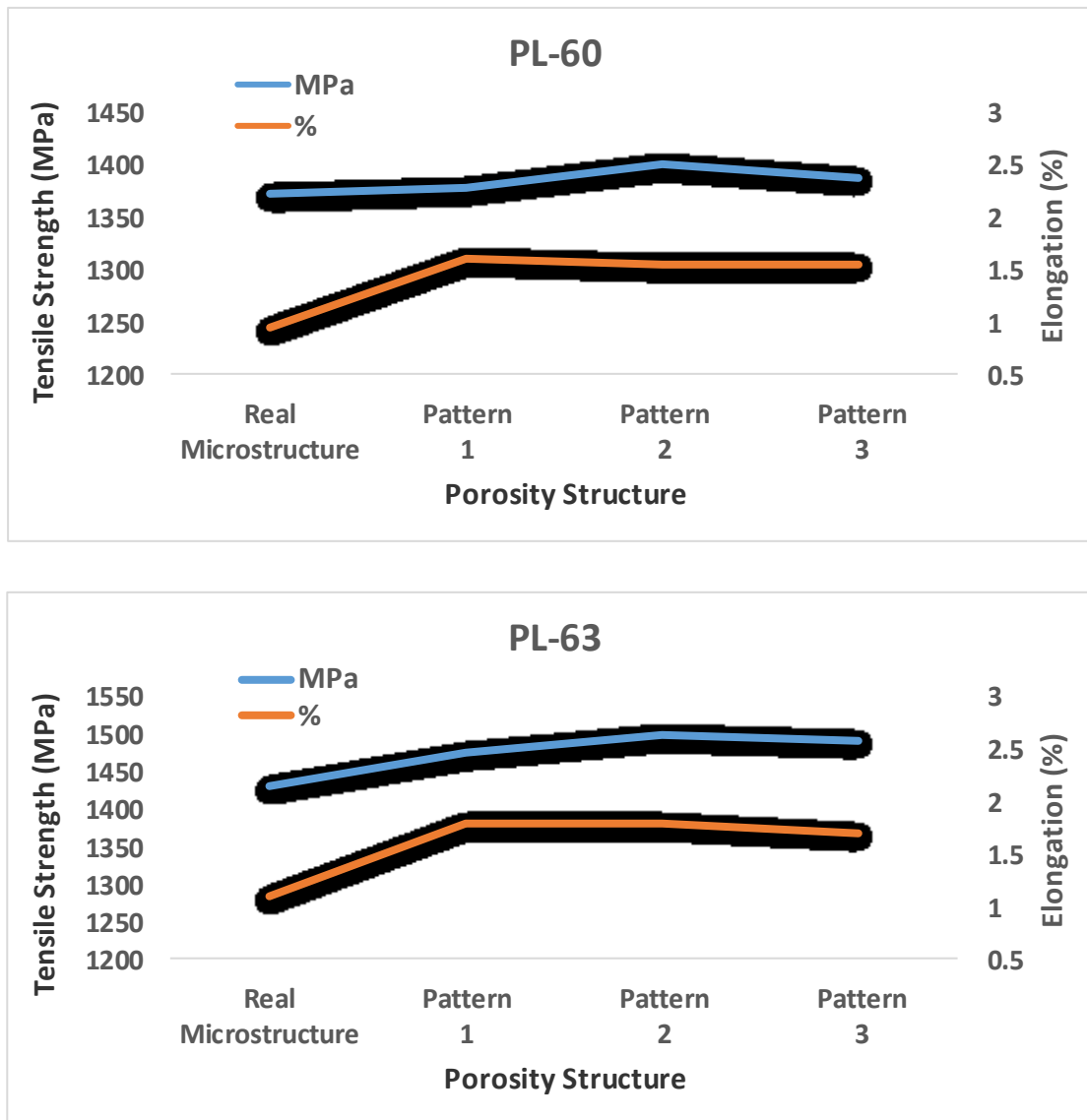
Fig. 2.14 Effect of pore reordering on mechanical properties of MIM steel. A negligible change in strength and ductility for both PL60 and PL63 models were observed.

2.5 SUMMARY

In this chapter, the effect of pore on the mechanical properties of MIM steel compact was systematically studied. The study consisted of two phases; experimentation work, and FEM simulation. All experimental data have been positively verified by the developed models. The following conclusions can be made based on the results of this chapter:

1. Powder loading of 63 vol% was an optimum fraction between 440C powder and binder system to form a feedstock in this work, and they offered better mechanical properties and microstructures.

2. Increasing powder loading resulted in lower pore fraction, and smaller average pore size.

3. Tensile strength and elongation increased with reduced porosity. It may attributed to smaller pore size and lower degree of pore clustering, which acts as a stress concentration for crack initiation.

4. Real microstructure-based FEM modeling showed that larger, irregular, and highly clustered pores contributed to significant stress localization, which resulted in premature failure at lower density. At higher density, the average pore sizes were smaller and more homogeneous distribution of plastic stress over a larger fraction of the matrix.

5. FEM modeling showed that plastic deformation developed gradually at the pore corners and highly clustered pores, especially for compacts with higher porosity.

6. When compacts at similar porosity level is considered, the factor of pore could be ignored due to minimum influences on the mechanical properties as confirmed by FEM data in this study.

2.6 REFERENCES

1)   A. Hadrboletz, B. Weiss: "Fatigue Behavior of Iron Based Sintered Material: A Review", International Mater., 42 (1997) 1-44.

2)   N. Chawla, S. Polasik, K.S. Narasimhan, M. Koopman, K.K. Chawla : "Fatigue Behavior of Binder-Treated P/M Steels", Int. J. Powder Metall., 37 (2001) 49-57.

3)   S.J. Polasik, J.J. Williams, and N. Chawla : "Fatigue Crack Initiation and Propagation in Binder-treated Powder Metallurgy Steels", Metall. Mater. Trans., 33A (2002) 73-81.

4)   K.D. Christian, R.M. German : "Relation between pore structure and fatigue behavior in sintered iron-copper-carbon", Intl J Powder Metal, 31 (1995) 51-61.

5)   U. Lindstedt, B. Karlsson, R. Masini : "Influence of porosity on the deformation and fatigue behavior of P/M austenitic stainless steel", Intl J Powder Metal, 33 (8) (1997) 49-61.

6)   A. John Sedricks : "Corrosion od Stainless Steels", Wiley, New York (1979).

7)   M.Q. Li, S.C. Ji : "Research oh High-Carbon Stainless Steel as Pump and Valve material: Effect of Heat-Treatment on Material's Microstructure and Performance", J. of Lanzhou University (Natural Sciences), 33 (4) (1997) 53-59.

8)   R.M. German, A. Bose : "Injection Molding of Metals and Ceramics", Metal Powder Industries Federation, Princeton, NJ, (1997) 231-239.

9)   G. R. White, R. M. German : "Dimensional Control of Powder Injection Molded 316L Stainless Steel Using in-situ Molding Correction", Advances in Powder Metallurgy and Particulate Materials, Metal Powder Industries Federation, Princeton, NJ, 5 (1993) 121-132.

10)   R.M. German, A. Bose : "Injection Molding of Metals and Ceramics", Metal Powder Industries Federation, Princeton, NJ, (1997) 3.

11)   E. Klar, P. K. Samal : "Powder Metallurgy Stainless Steels: Processing, Microstructures, and Properties", ASM International (2007) 20.

12)   R.M. German : "Powder Metallurgy of iron and steel", Wiley-interscience (1990) 73-78.

13)   G. Aggarwal, S.J. Park, I. Smid, R.M. German : "Master Decomposition Curve for Binders Used in Powder Injection Molding", Metallurgical Transactions A, 38 (3) (2007) 606-614.

14)   H. Miura, S. Yasunaga, N. Ogasawara, S. Ando, T. Honda : "Metal Injection Molding Process of martensitic stainless Steels", J. Jpn. Soc. Powder Powder Metallurgy, 41 (1994) 1071-1074.

15)   K. S. Hwang, Y. M. Hsieh : "Comparative Study of Pore Structure Evolution During Solvent and Thermal Debinding of Powder Injection Molded Parts", Metallurgical and Materials Transactions A 27A (1996) 245-253.

16)   Y.-L Fan, K.-S. Hwang, et al. : "Minimum Amount of Binder Removal Required during Solvent Debinding of Powder-Injection-Molded Compacts", Metallurgical and Materials Transactions A 40A (2009) 768-779.

17)   Y.-L. Fan, K.-S. Hwang, et al. : "Improvement of the Dimensional Stability of Powder Injection Molded Compacts by Adding Swelling Inhibitor into the Debinding Solvent", Metallurgical and Materials Transactions A 39A (2007).

18)   P. K. Samal, J.C. Valko, J.D. Pannell : "Processing and Properties of PM 440C Stainless Steel", Advances in Powder Metallurgy & Particulate Materials–2009, Part 7 (2009) 112-121.

19)   K.M. Vedula, R.W. Heckel : "Modem Developments in Powder Metallurgy", Metal Powder Industries Federation, Princeton, NJ (1981).

20)   W.A. Spitzig, R.E. Smelser, O. Richmond : "The Evolution of Damage and Fracture in Iron Compacts with Various Initial Prosities", Acta Metall., 36 (1988) 1201-1211.

21)   G. Straffelini, A. Molinari : "Evolution of Tensile Damage in Porous Iron", Mater. Sci. Eng. A, 334 (2002) 96-103.

22)   R.J. Bourcier, D.A. Koss, R.E. Smelser, O. Richmond : " The Influence of Porosity on the Deformation and Fracture Alloys", Acta Metall., 34 (1986) 2443-2453.

CHAPTER 3

Effect of Heterogeneous Microstructure on the Mechanical Properties of Superhigh Strengthening MIM Fe-Ni Steel Compacts

3.1 INTRODUCTION

Through recent technological advancement, metal injection molding (MIM) process is remarkably capable to offer perfect net shape and almost near full dense metal component. This benefit even more extremely appreciated when high-performance steels are utilized to the process, where other processes would be difficult or impossible to fabricate the parts at similar production cost.

In this study, Fe-Ni low alloy steels is subjected to the MIM process in order to fabricate superhigh strengthened Fe-Ni steel compacts. The steel compact has microstructural morphology, which are multiphase and heterogeneous in nature [1-2]. The mixed elemental-based powder for both Fe and Ni elements was utilized to enhance these effects.

In this study, all superhigh strengthened Fe-Ni steel compacts obtained experimentally were characterized by heterogeneous microstructure with porosity (at least 4-5 %). This heterogeneity was particularly derived from the variation of Ni concentration throughout the matrix. From view of metallic phase, this heterogeneous microstructure consisted of a complicated network of various phases of martensite. To be brief, the network was structured by the Ni rich martensite and surrounded by the tempered martensite.

The objective of this chapter is to experimentally investigate the unique correlation between variation of Ni distributions throughout superhigh strengthened Fe-Ni steel compacts, and the mechanical properties. Thus, in order to have a thorough understanding and careful control of the microstructure, three important aspects; different Ni mean particle sizes, various Ni addition contents, and sintering conditions (especially the temperature and time) were selected and comprehensively examined. The experimentation works will be described and discussed in detail.

3.2 EXPERIMENTAL METHOD

Fine carbonyl iron powder with mean particle size of 4.4 µm (Fukuda Metal Foil & Powder Co., Ltd. Japan) was utilized as a base powder. Whereas, three ultra high pressure water-atomized Ni powders (Mitsubishi Steel Mfg. Co., Ltd. Japan) with mean particle size of 6, 16, and 24 µm were used as an alloy powder. They are named f (fine), m (medium), and c (coarse) in this study, respectively. The SEM images of these powders are shown in Fig. 3.1. Also their chemical compositions are given in Table 3.1. Five different compact conditions were prepared. Ni mean particle sizes, and addition of Ni content (mass%) were varied as shown in Table 3.2.
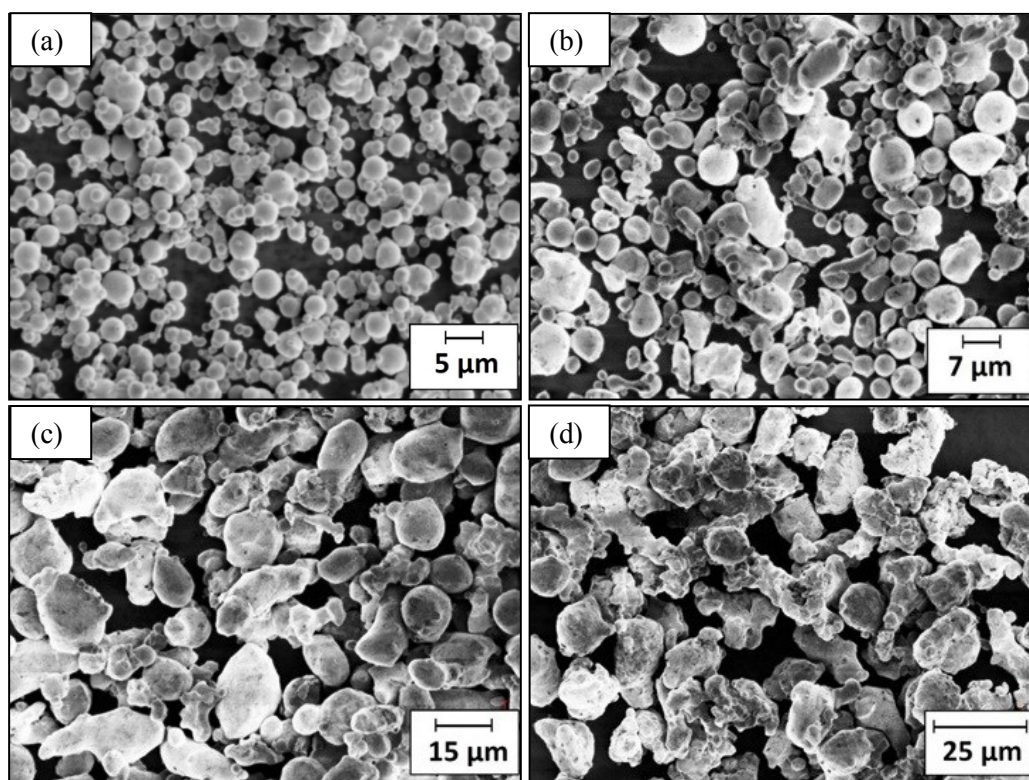
Fig. 3.1 SEM morphology of base and alloy powders a) fine iron, b) fine Ni, c) medium Ni, and d) coarse Ni particles.

Table 3.1 Chemical composition (mass%) of iron and nickel powders.

	C	Si	Mn	Fe	Ni	O
Fe	0.76	-	-	Bal	-	0.30
Ni	0.01	1.10	0.19	0.28	Bal	0.001

Table 3.2 Symbols of prepared compacts in this study.

Ni mean particle size (μm) / Ni (mass%)	4	6	8
Fine (6)	Fe-4Ni-f	Fe-6Ni-f	Fe-8Ni-f
Medium (16)	-	Fe-6Ni-m	-
Coarse (24)	-	Fe-6Ni-c	-

Binder material was consisted of 69 mass% paraffin wax (PW), 20 mass% atactic polypropylene (APP), 10 mass% carnauba wax (CW), and 1 mass% stearic acid (SA). After Fe and Ni powders were mixed by a V-blender for 2 hours, the mixed powder (64 vol%) and the binder material (36 vol%) were kneaded by a mixer (5DMV-01-rr, Dalton Co., Ltd.) at 150 ℃ for 1.5 hours. All feedstock was injection molded using an injection molding machine (JC50SA II, Japan Steel Works, Ltd.) into flat-bar tensile green compacts; the gauge length was 40 mm, and width and thickness were 7.5 and 4 mm as shown in Figs. 2.4 (chapter 2), respectively.

The extraction of binder from the green compacts began with solvent debinding in vaporized heptane at 50 ℃ for 4 hours then followed by thermal debinding in argon atmosphere where heating at 2 ℃/min up to 600 ℃ for 1 hour. Subsequently, the debound compacts were pre-sintered at 900 ℃ for 0.5 hour prior to sintering at three temperatures of 1200, 1250, and 1350 ℃ for 1 hour or 4 hours in vacuum at 10^{-1} Pa and were remained in vacuum for cooling to room temperature in the same furnace (VHLgr20/20/20, Shimadzu Mectem, Inc.). The sintered compacts were austenized in argon gas flow at 900 ℃ for 0.5 hour before oil-quenched to room temperature. The compacts were finally tempered by reheating in argon gas flow for 2 hours at 200 ℃. Sintered density was measured by Archimedes water immersion technique. The carbon content was determined by carbon combustion analyzer. The mappings of Ni distribution were accomplished by electron probe microanalyzer (EPMA-1600, Shimadzu Corporation). The tensile properties were obtained by a universal tensile tester equipped with extensometer (AG-X, Shimadzu Corporation).

3.3 RESULTS AND DISCUSSION

3.3.1 Experimental Data

After sintering, density of each compact was higher than 7.50 g/cm³, which is 95 % of theoretical density, as shown in Fig. 3.2. The highest relative density was 98 % attained by compact sintered at 1350 ℃ for 4 hours. The carbon contents for all

tempered steels were around 0.4 mass%. Due to effective blending and mixing processes, all Ni particles have been successfully dispersed throughout the green compacts as confirmed by EPMA mappings. Ni element mappings on green compacts are shown in Fig. 3.3.

Figure 3.4 shows representative mappings of Ni element for all compacts. Element mappings by EPMA analysis were carried out on as-tempered compact. The mappings were organized into three groups; Ni mean particle size, Ni content (mass%), and sintering condition (temperature and time) as shown in Figs. 3.4 (a), (b), and (c) respectively. All mappings confirmed that there were peaks and valleys on the Ni networks throughout the compact matrix. As the Ni particle size and the Ni content (mass%) increased, the peaks were getting higher as shown in Figs. 3.4 (a) and (b). In contrast, the peaks were decreased when sintering temperature increased due to better Ni diffusion into surrounding matrix.

The 3% Nital reagent was used to reveal the martensite crystalline structure of the compact in this study. The as-sintered compact has been identified to contain ferrite, bainite, pearlite, and Ni rich phase. Unlike other phases, the Ni rich phase was found only in three compact conditions; Fe-6Ni-m, Fe-6Ni-c, and Fe-8Ni-f as shown by arrows in Fig. 3.5 (a). After heat-treatment, the microstructure of as-sintered compact has been transformed into two different regions; the bright martensite region which was surrounded by tempered martensite region as shown in Fig. 3.5 (b). These bright and tempered martensite regions were observed in the microstructure of all compacts. The bright martensite region was originated from the parent phase of Ni rich phase or higher Ni content region in as-sintered compact. The boundary between the bright and tempered martensite regions became clearer when Ni particle increases in size. In addition, Fig. 3.5 (c) shows that the bright regions seem to grow with the increase in Ni content, in the case of constant Ni particles size.
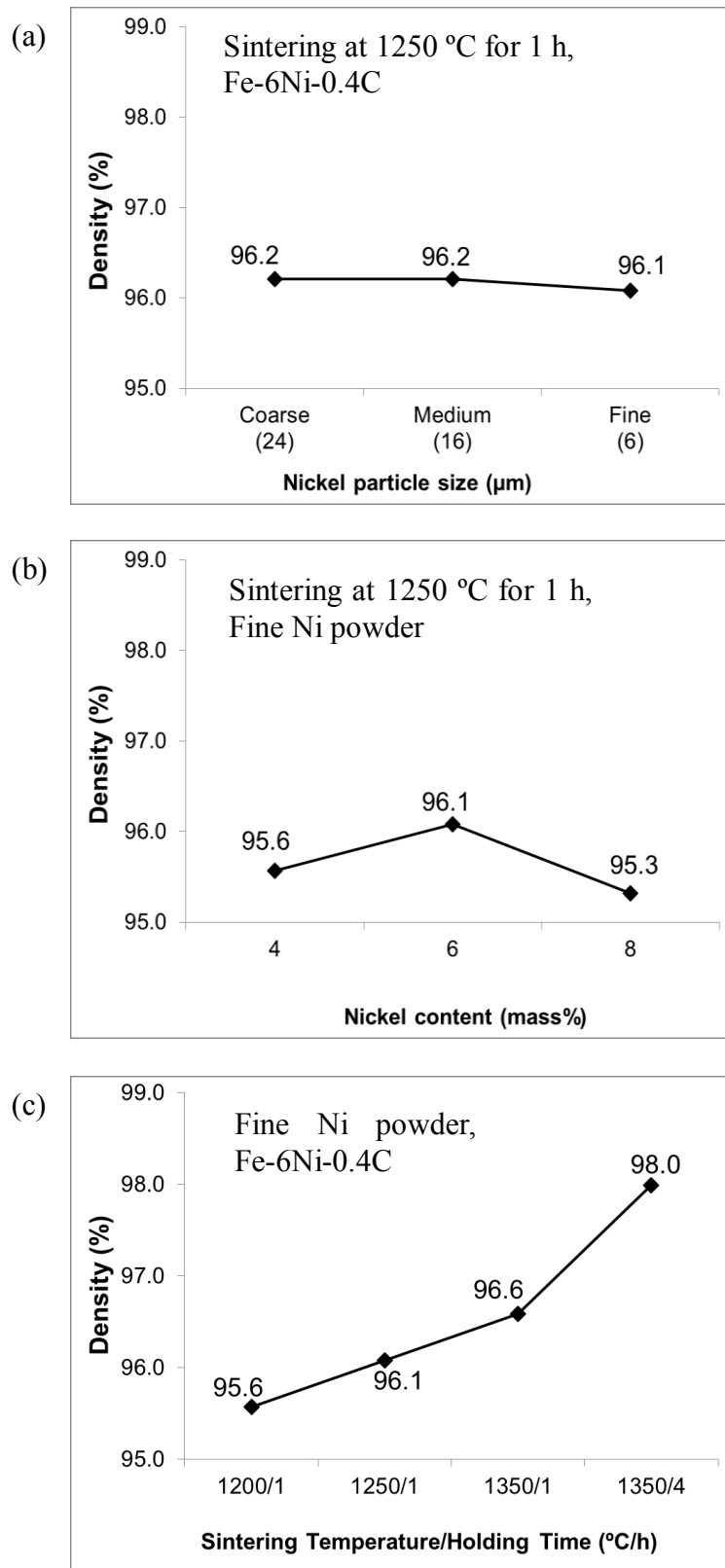
Fig. 3.2 Effect of (a) Ni particle size, (b) Ni content, and (c) sintering temperature and time on the Fe-Ni steel compacts.
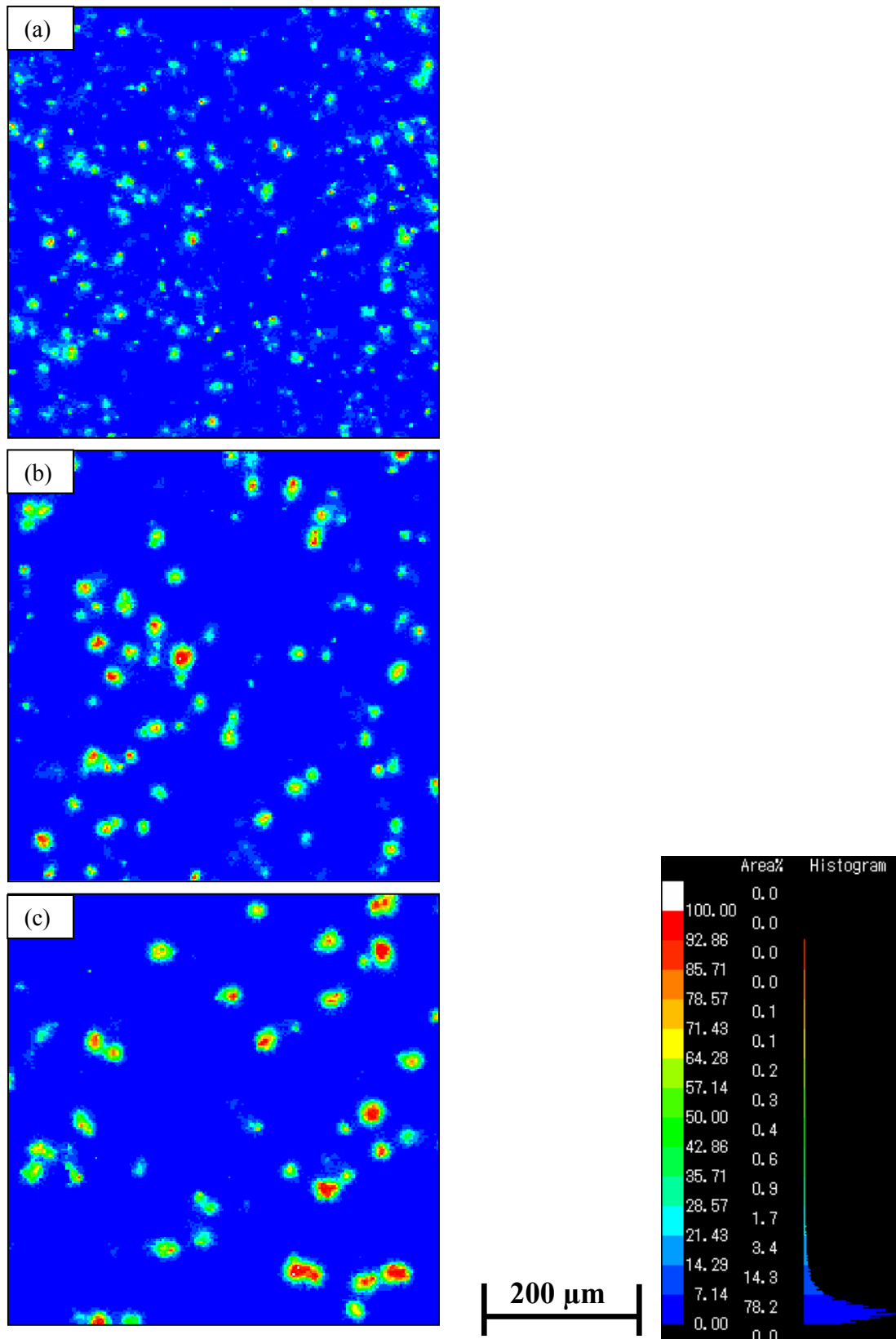
Fig. 3.3 Representative of Ni element mapping by EPMA analysis for green compact of Fe-Ni steel compacts with a) Fine b) Medium, and c) Coarse Ni powder.
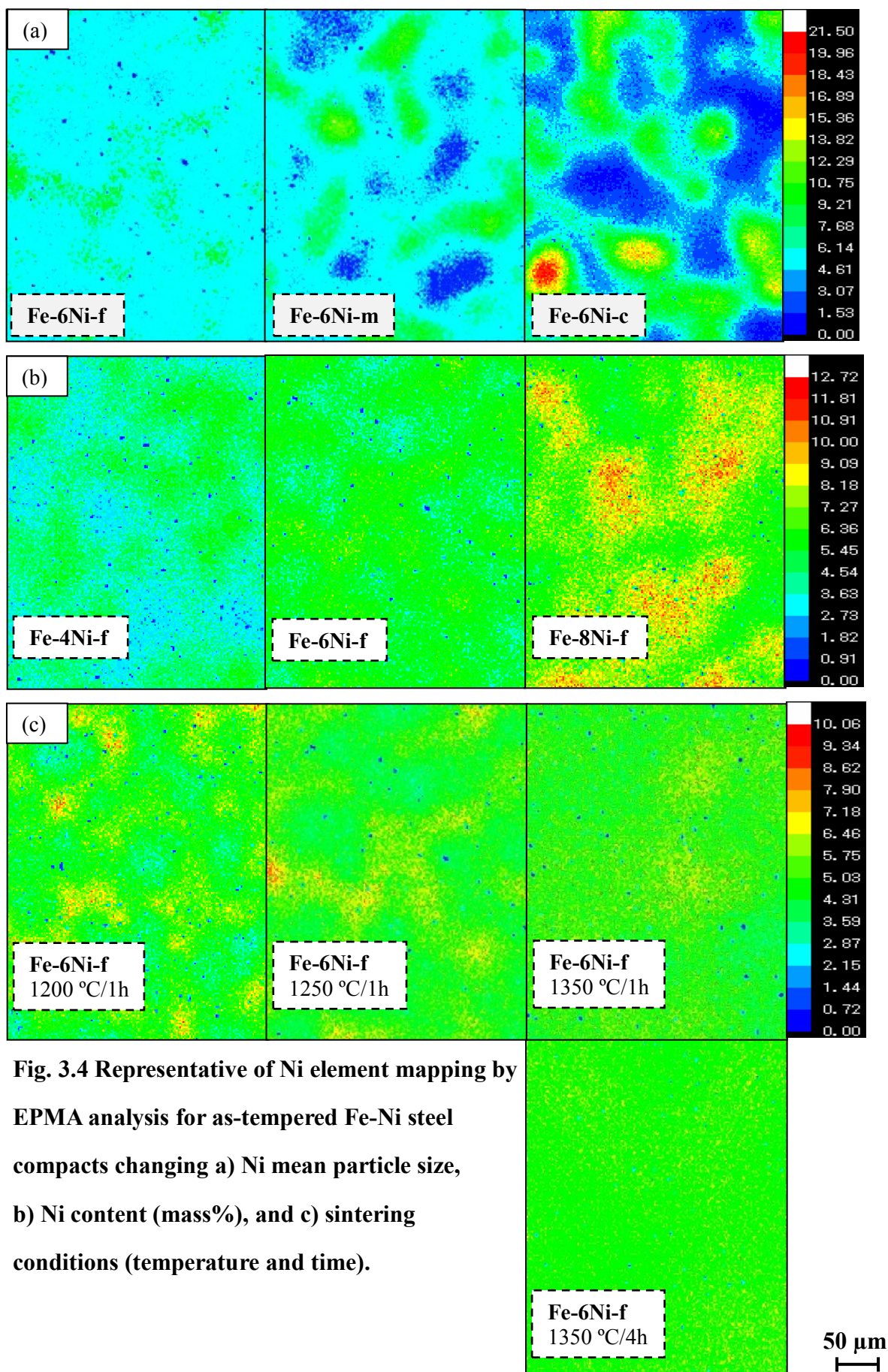
Fig. 3.4 Representative of Ni element mapping by EPMA analysis for as-tempered Fe-Ni steel compacts changing a) Ni mean particle size, b) Ni content (mass%), and c) sintering conditions (temperature and time).
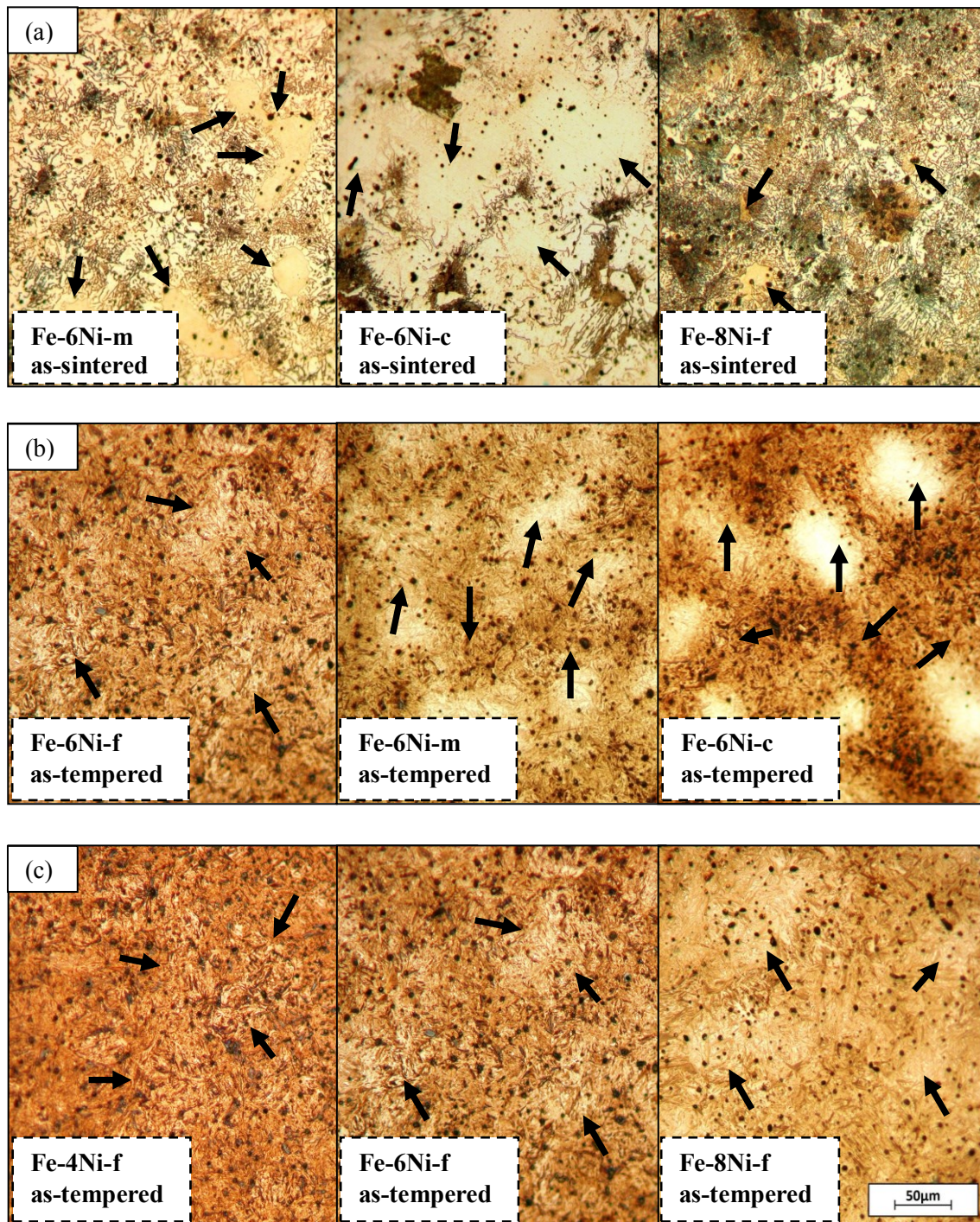
Fig. 3.5 Representative of optical microstructure for various Fe-Ni steel compacts a) as-sintered compacts contain Ni rich phase, b) as-tempered compacts of different Ni particle size, c) as-tempered compact of different Ni content (mass%) sintered at 1250 ºC for 1 hour in vacuum atmosphere. The arrow shows the bright martensite region.

As shown in Fig. 3.6, the micro-Vickers hardness in tempered martensite regions were higher than those of Ni bright martensite for all three conditions; fine, medium, coarse of Fe-6mass%Ni steel compacts. As the size of Ni particle increased, the hardness for both the bright and the tempered martensite were declining. Lower hardness value offered by the bright region was due to higher volume of retained austenite. In contrast, the tempered martensite region found to contain lower volume of the retained austenite [3].
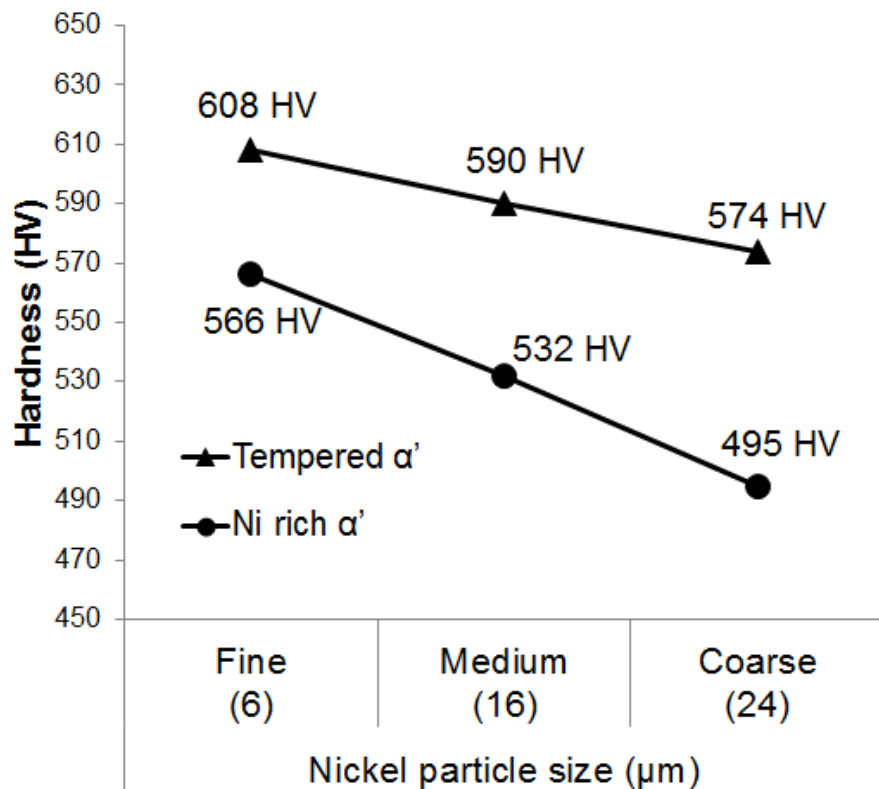
Fig. 3.6 Hardness of bright and dark (tempered) martensite regions for Fe-6Ni-f, Fe-6Ni-m, and Fe-6Ni-c steel compacts sintered at 1250 ºC for 1 hour in vacuum atmosphere.

The mechanical properties of tensile strength and elongation of the tempered compacts were compared into three ways; Ni mean particle size, Ni content (mass%), and sintering conditions (temperature and time) as shown in Fig. 3.7, 3.8, and 3.9 correspondingly. Figure 3.7 shows the tensile strength and elongation for Fe-6Ni steel

compacts with fine, medium, and coarse Ni powders. The compacts with 6 mass% of fine Ni powder shows the best mechanical properties compared to the compacts with 4 and 8 mass% Ni content as shown in Fig. 3.8. The trend illustrates differently when the data was compared based on different Ni content from 4 to 8 mass% where the performance were increased to their peak at 6 mass% Ni content before plunged to lower mechanical properties at 8 mass% Ni. In order to study the effect of sintering temperature, the 6 mass% fine Ni powder compacts were sintered at three different sintering temperatures; 1200, 1250, and 1350 ºC. Both tensile strength and elongation were improved when sintering temperature increased from 1200 to 1250 ºC. Although, the tensile strength seems to increase a little from 2040 to 2055 MPa when sintered at 1350 ºC, the elongation was decreased from 8.1 into 5.1 %.
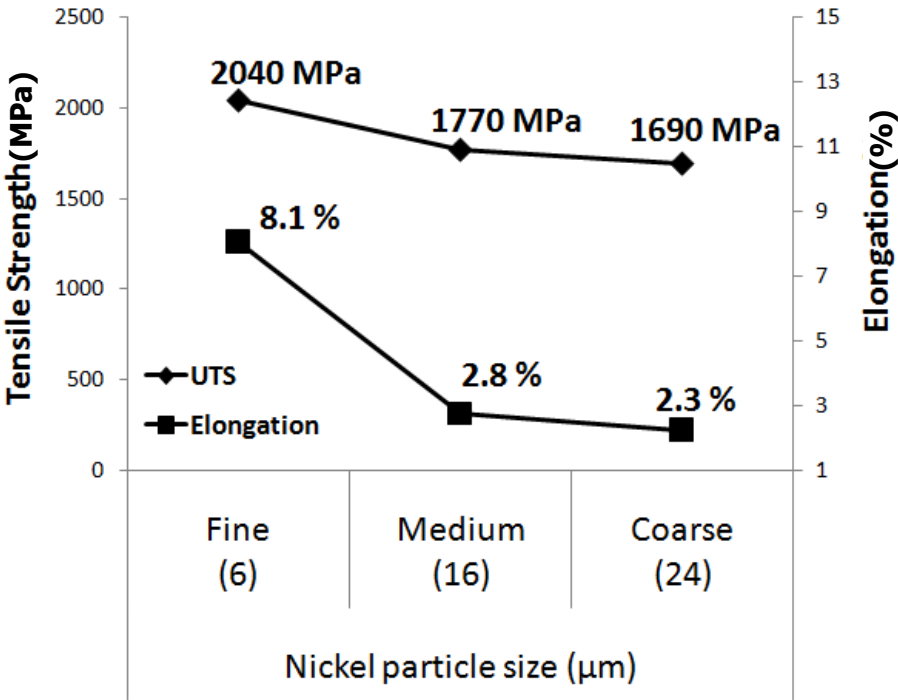
Fig. 3.7 The ultimate tensile strength and elongation of as-tempered Fe-6Ni-f, Fe-6Ni-m, and Fe-6Ni-c compacts at 1250 ºC sintering temperature for 1 hour in vacuum atmosphere.
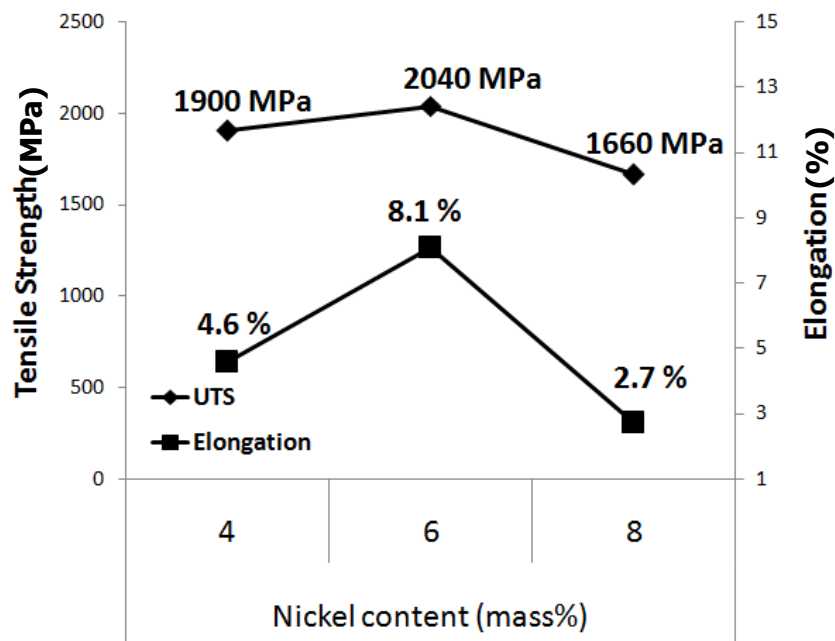
Fig. 3.8 The ultimate tensile strength and elongation of as-tempered Fe-4Ni-f, Fe-6Ni-f, and Fe-8Ni-f compacts sintering at 1250 ºC for 1 hour in vacuum atmosphere.
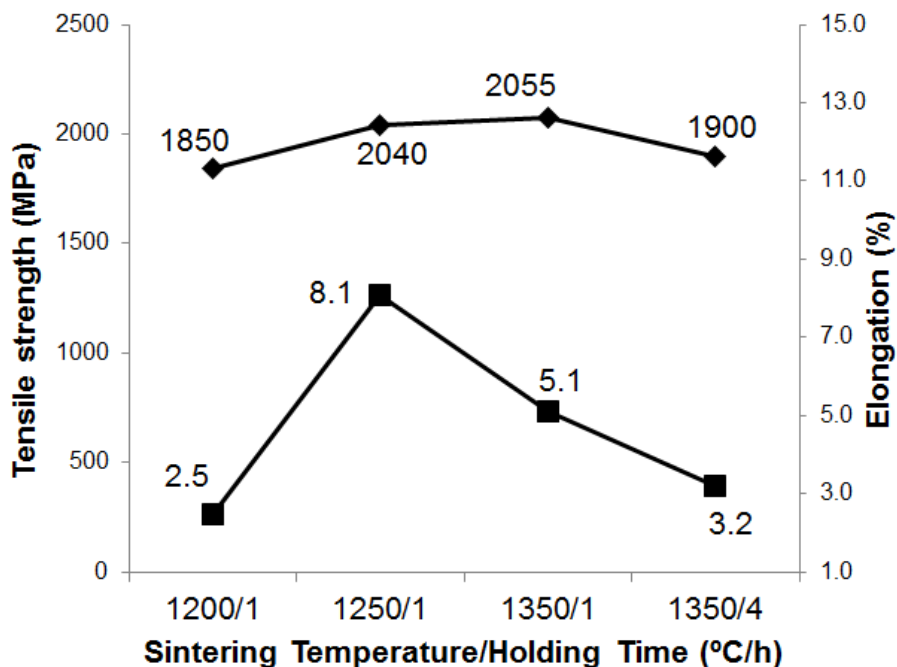
Fig. 3.9 The ultimate tensile strength and elongation of as-tempered Fe-6Ni-f at different sintering temperature of 1200, 1250, and 1350 ºC for 1 and 4 hours in vacuum atmosphere.

3.3.2 Nickel Diffusivity

Topography of Ni element by EPMA analysis has confirmed that compacts with fine Ni powder demonstrates excellent Ni diffusion into the surrounding matrix as shown in Fig. 3.4 (a). There were some Ni free regions in Fe-6Ni-c steel matrix. The Fe-6Ni-f steel compacts, where Ni effectively diffused throughout the matrix offered superior mechanical properties over Fe-6Ni-m and Fe-6Ni-c compacts. As shown in Fig. 3.3, no severe agglomeration of the Ni particles has been sighted in the green compacts as well as in the pre-sintered compacts for fine, medium, and coarse Ni particle sizes.

In general, the diffusivity of Ni could be improved in two ways; higher sintering temperature and longer sintering time. Since Ni effective diffusion range was short, fine powders should be used to minimize such the problem. Detailed examination on Ni element topography of Fe-6Ni-f compact by EPMA analysis has confirmed the existence of Ni peaks and valleys throughout the matrix. The average of maximum and minimum Ni spots for Fe-6Ni-f compacts were 9.3 and 2.5 mass% correspondingly. This large variations up to 6.8 mass% between Ni peaks and valleys proved that the microstructure of Fe-6Ni-f steel compacts was not homogeneous but heterogeneous. The variation became even bigger for the Fe-6Ni-m and the Fe-6Ni-c compacts with 11.3 and 20.1 mass%, respectively.

The efforts to characterize the Ni diffusivity phenomenon continued on the Fe-6Ni-f compact through two complementary sintering temperatures which were lower and higher than initial temperature of 1250 °C. The compacts sintered at 1350 °C were more homogeneous compared to the lower temperatures. Variation between peak and valley of Ni contents in the compacts sintered at 1200 and 1350 °C were 8 and 6 mass %, respectively. Although the compact sintered at 1350 °C looked more homogeneous, the variations of Ni distribution has been remained, which means the structure was still in heterogeneous state.

When the holding time during sintering was increased to 4 hours at 1350 °C, more homogeneous state was achieved as shown in the right-bottom of Fig. 3.4. The variation among peak and valley points was only 2 mass%. From Fig. 3.9, although the strength

increased a little due to densification at higher sintering temperature, the ductility has dramatically degraded as a result of microstructure coarsening (grain growth) [4].

3.3.3 Nickel Rich Phase

From the optical microstructure as shown in Fig. 3.5, no Ni rich phase was found on the Fe-6Ni-f compact regardless of their best performance. However, yet the higher Ni regions were clearly found on the compact by EPMA analysis as shown in Fig. 3.4. Therefore, further detailed analysis of Ni element topographies and optical microstructures were performed by using the image analyzing software. The Ni rich phase can be certainly observed under optical microscope when the amount of localized Ni content was more than 10 mass%. The highest peak point for Ni content in Fe-6Ni-f compact was found around 8.5 mass%. This is a reason for no Ni rich phase has been found in Fe-6Ni-f and some other compacts under an optical microscope.

The higher Ni content regions (including Ni rich phase) transformed into bright martensite, whereas lower or no Ni content regions became tempered martensite (dark looked region) when subjected to heat treatment as shown in Figs. 3.5 (b) and (c). The bright martensite region of Fe-6Ni-f compact mainly composed of Ni martensite structure. However, as Ni powder getting coarser, the region became dominated by greater amount of meta-stable austenite which bordered by Ni martensite before surrounded by tempered martensite of steel matrix [1-2,5-6]. This observable fact is supported by micro-Vickers hardness data as shown in Fig. 3.6 where the hardness of bright martensite region for each compact has decreased with increasing in Ni particle size. Also, the Ni concentration in the regions has been increased with increases in Ni particle size as well as in Ni content. The nature of three-dimensional (3D) network structure was schematically shown in Fig. 1.1 (chapter 1).
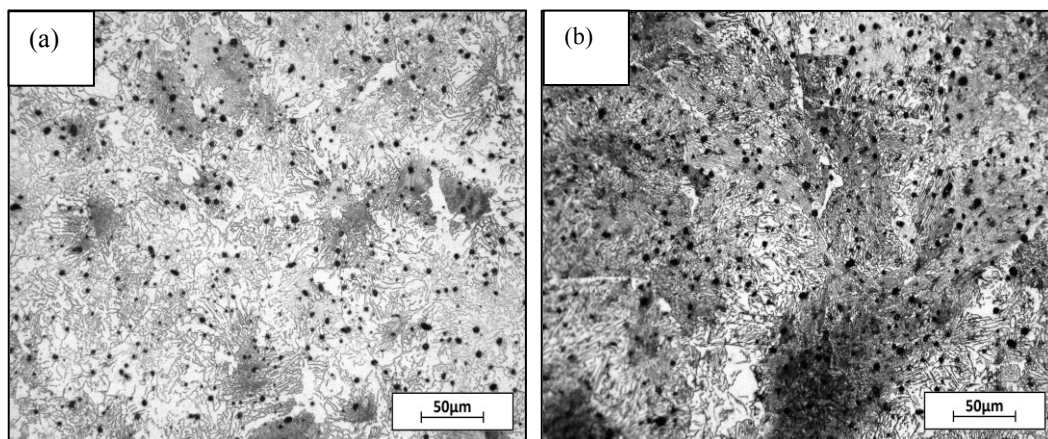
3.3.4 **Mechanical Properties**

Figures 3.7 and 3.9 show the ultimate tensile strength and elongation of all compacts obtained in this study. Tempered Fe-6Ni-0.4C compact sintered at 1250 ℃ for 1 hour using fine Ni powder demonstrated the best combination of mechanical properties achieved with 2040 MPa strength and 8.1 % elongation. Compared to the compacts using coarse and medium Ni powders, the compact using fine Ni powder showed less heterogeneity. In Fig. 3.7, highly heterogeneous structure (using coarse Ni powder) has offered unfavorable mechanical properties with ultimate tensile strength of 1690 MPa and elongation of 2.3 %.

Since the compacts with fine Ni powder showed superior mechanical performance over medium and coarse, more attention has been set for the fine Ni powder-based compacts. The solid solution strengthening effects [5] by Ni element in the steel matrix of Fe-Ni steel compact have been enhanced with additions of Ni mass% as shown in Fig. 3.8. The Fe-4Ni-f compact shows strength of 1900 MPa, 4.6 % elongation, and 55 HRC. The mechanical properties has been improved when another 2 mass% Ni added to Fe-6Ni-f steel compact. Nevertheless, addition of 8 mass% Ni shows undesired trends where the properties has been diminished into 1660 MPa in UTS, 2.7 % elongation, and 53 HRC. Therefore, Fe-Ni steel compact with fine 6 mass% Ni is a critical limit for Ni strengthening into steel matrix which is consistent with Miura's findings [1,5,6].

As shown in Fig. 3.9, the highest ultimate tensile strength was obtained by sintering at 1350 ℃ for 1 hour. However, elongation has been dropped to 5.1 %. Also, the mechanical properties were decreased when a prolonged holding time of 4 hours was employed at 1350 ℃. The higher sintering temperature and longer sintering time possibly cause the grain growth which deteriorates the mechanical properties, in addition to homogeneity. Figures 3.10 a) and b) show the optical microstructure images of sintered compacts at 1250 and 1350 ℃ for 1 hour. The average grain size for both compacts were 25 and 73 μm, respectively. The mechanical properties were affected by not only the grain size but also the homogenization of the microstructure.

The mechanical properties of heterogeneous structured compact was depreciated as it promoted into homogenous state [2-3,6]. In the following chapter, simulated results are shown to evaluate how the heterogeneity affects on the mechanical properties.

Fig. 3.10 Optical microstructures of Fe-6Ni-0.4C compacts using fine Ni powder sintered at (a) 1250 ºC , and (b) 1350 ºC for 1 hour.

3.3.5 Transformation Induced Plasticity (TRIP)

Miura and other researchers reported that the excellent mechanical properties could also be attributed to the martensitic transformation-induced plasticity (TRIP) effect in the retained austenite phase [1-3,5-6,7-13]. As shown in Fig. 3.5 (b), the optical microstructure has demonstrated that the retained austenite and martensite are distinguishable etching with 3 % Nital reagent.

Figure 3.11 shows the content of retained austenite in the Fe-6Ni-f compact before and after tensile test. By the TRIP effect, the metastable retained austenite in the bright Ni rich phase transformed into martensite by the deformation subjected during uniaxial tensile testing. Thus, volume fraction of martensitic structure in the region of brighter Ni rich phase increased almost 10 vol%; it causes the Ni rich martensite region become harder than the initial tempered martensite region as confirm by hardness data in Fig. 3.12.

This is how the retained austenite can affect the mechanical properties. The retained austenite at interlath layers of Ni rich martensitic structure especially on the Fe-6Ni-f compact matrix could increase the strength by enhancing the ability of lath boundaries to obstacle dislocation movement [7]. At the same time , the retained austenite could also enhance the elongation due to the TRIP effect [12]. So, the higher volume fraction of the retained austenite should correlate with improved mechanical properties.

However, although Fe-6Ni-m and Fe-6Ni-c compacts have high volume of retained austenite, they are stable austenite at room temperature due to high Ni concentration, which more than 10 vol%. As a result, the TRIP effect were much lesser in these two steel compacts.
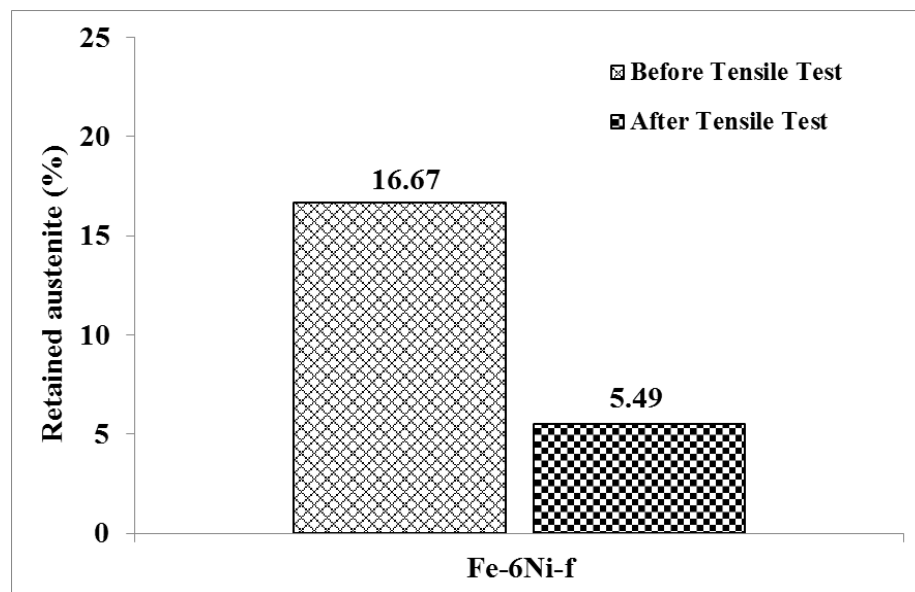
Fig. 3.11 Volume fraction of retained austenite in the Fe-6Ni-f compact for before and after tensile testing sintered at 1250 ºC for 1 hour.
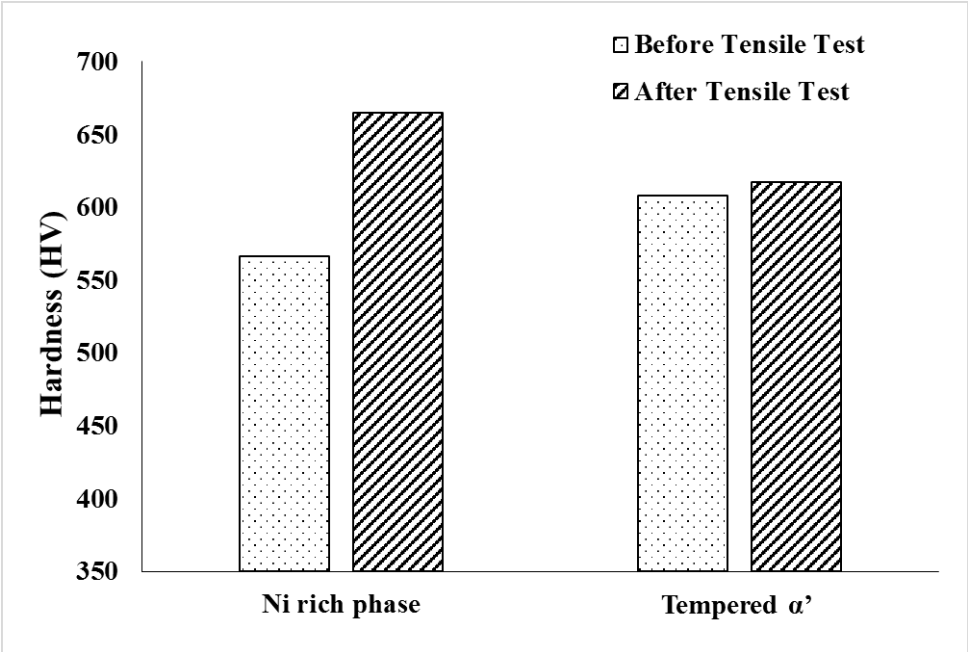
Fig. 3.12 Hardness of Ni rich phase and tempered martensite regions of Fe-6Ni-f compact for before and after tensile testing sintered at 1250 ºC for 1 hour.

3.3.6 Data Comparison

The detailed comparison between Fe-6Ni-f compact and other reported data for low alloy steels group are shown in Table 3.3. It is worth to note that the Fe-6Ni-f steel compact in this study shows the highest strength and the most excellent ductility among the reported data to date in MIM low alloy steel category. These outstanding mechanical properties which are comparable to wrought material could be attributed to fine heterogeneously distribution of smaller particle size of Ni which later strengthen the compact by heat treatment.

Table 3.3 Data comparison between Fe-6Ni-f, other MIM compacts,

press-tempered, and wrought low alloy steels [5,15-17].

Material (Fabrication)	Condition	Yield Strength (MPa)	Ultimate Tensile Strength (MPa)	Elongation (%)	Hardness HRC
Fe-6Ni-f (MIM) *elemental powders*	as-sintered	315	640	11	-
	as-tempered	**1250**	**2040**	**8**	**56**
Fe-6Ni-0.5Mo -0.2Mn (MIM) [5] *elemental powders*	as-tempered	N/A	1985	5	52
4140 (MIM) [15] *alloy powders*	as-tempered	1240	1650	5	46
4605 (MIM) [16] *alloy powders*	as-tempered	1480	1655	2	48
FLC-4805 (Pressed) [16] *elemental powders*	as-tempered	N/A	1280	<1	39
Fe-18Ni-8Co-4.5 Mo-0.5Ti-0.1Al (Wrought) [17]	as-aged	1700	1800	8	48
4340 (Wrought) [17]	as-tempered	1860	1980	11	53
4340+1.6Si (Wrought) [17]	as-tempered	1650	2140	7	54
8640 (Wrought) [17]	as-tempered	1670	1810	8	55

3.4 SUMMARY

This chapter covers all experimentation works of superhigh strengthened Fe-Ni steel compact. The tempered Fe-6Ni-0.4C compact with fine mixed elemental powders achieved remarkably high ultimate strength of 2040 MPa, yield strength of 1200 MPa, hardness of 56 HRC, and excellent elongation of 8.1 %. The correlation between Ni distributions in the matrix and the mechanical properties of superhigh strengthened Fe-Ni steel compacts has been successfully investigated. Variation of Ni concentration throughout the compact matrix was established to be one of major roles for obtaining excellent mechanical properties of superhigh strengthened Fe-Ni steel compact.

Better diffusivity of the Ni element into surrounding Fe matrix was also found to be essential to guarantee good mechanical properties of the compact as confirmed experimentally. From series of Ni element mapping by EPMA analysis, all compacts of superhigh strengthened Fe-Ni steel compacts were subjected to variation of Ni concentration throughout the matrix; its means that all compacts obtained in this study were showed heterogeneous microstructure. The compact characterized by complete Ni diffusion and at smaller variation of Ni concentration demonstrated better combination of the mechanical properties.
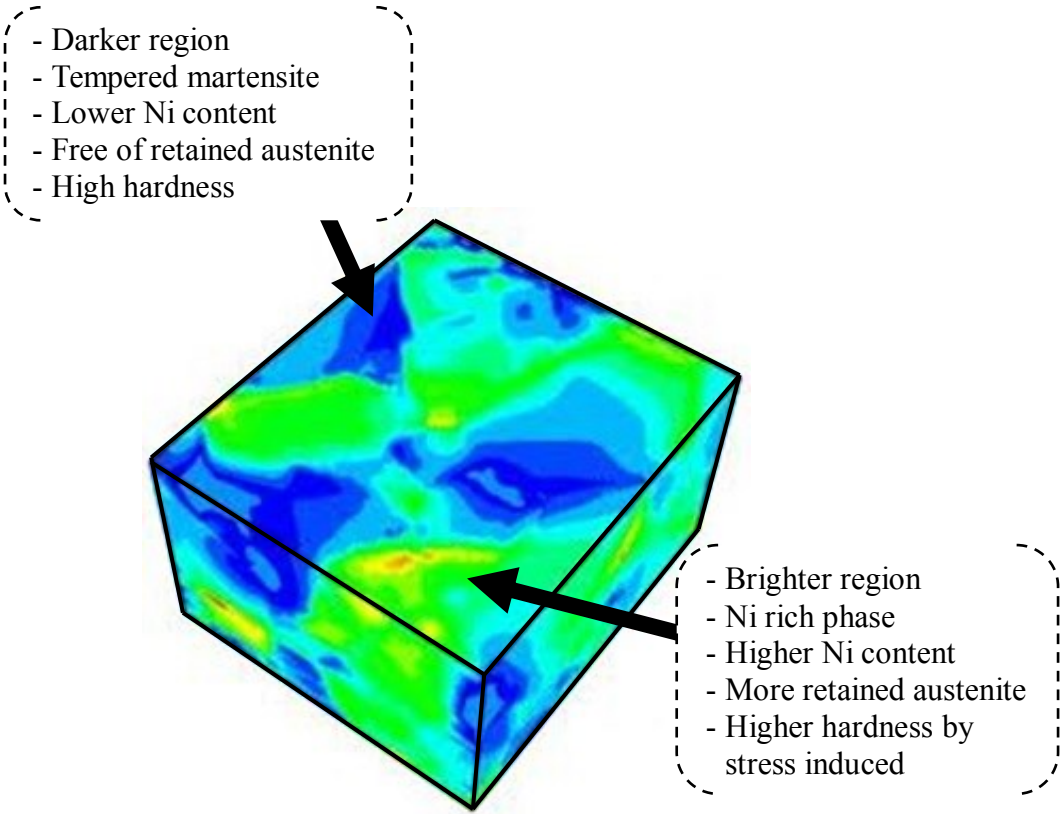
After heat treatment, the heterogenous microstructure of superhigh strengthened Fe-Ni steel compacts were characterized by complex martensite network, where softer bright martensite (Ni rich martensite) was surrounded by harder tempered martensite throughout the matrix as confirmed through experimental data in this study. The softer region of bright martensite was contained relatively higher Ni content, whereas, harder dark martensite region contained lower concentration of Ni.

When mechanical deformation was subjected by the tensile test, this network has been efficiently transformed into different complex martensitic network where the brighter martensite became harder than the tempered martensite. This is possibly due to the martensitic transformation-induced plasticity (TRIP) effect. This unique characteristic is attributed to the presence of a metastable austenitic phase in the

microstructure at room temperature.

Therefore, additional facts about heterogeneous microstructure model obtained in this study can be schematically summarized in Fig. 3.13. The model represents comprehensive condition of the superhigh strengthened Fe-Ni steel compact after subjected to tensile testing. Also, careful control of the dispersion state of the Ni concentration throughout the matrix is a key factor for their excellent properties.

In the following chapter, the FEM simulation is used to evaluate the effect of the heterogeneous the mechanical properties. The FEM was enhanced from pores structure model shown in chapter 2. Also, all constructed models in the following chapter will be based on deformational state (after tensile test). The modeling is intensively working on the two key regions as discussed in the present chapter; the higher Ni region, and the matrix (lower Ni region).

- Darker region
- Tempered martensite
- Lower Ni content
- Free of retained austenite
- High hardness

- Brighter region
- Ni rich phase
- Higher Ni content
- More retained austenite
- Higher hardness by stress induced

Fig. 3.13 Schematic diagram of 3D network of Ni elemental mapping of superhigh strengthened Fe-Ni steel microstructure.

3.5 REFERENCES

1)   M. Matsuda, H. Miura : "Mechanical Properties of Injection Molded Fe-6%Ni-0.4%C Steels with Varying Mo Contents of 0.5 to 2%", Metals and Materials International, 9 (2003) 537-542.

2)   H. Miura, S. Mitomi, S. Ando, T. Honda : "Effect of homogeneous and heterogeneous structure on the properties of sintered alloy steels by MIM", J. Jpn. Soc. Powder Powder Metallurgy, 42 (1995) 378-382.

3)   H. Miura : "High Performance Ferrous MIM Components Through Carbon and Microstructural Control",   Materials and Manufacturing Processes, 12 (1997) 641-660.

4)   H. Zhang, R.M. German : "Homogenization   and   Microstructure Effects on   the   Properties   of   Injection   Molded   Fe-2Ni   Steel", Metallurgical and materials Transactions A, 23 (1992), 377-382.

5)   H. Miura, M. Matsuda : "Superhigh Strength Metal injection Molded Low Alloy Steels by In-Process Microstructural Control", Material Transactions, 43 (2002) 343-347.

6)   H. Miura, M. Matsuda : "Ultrahigh strengthening sintered low alloy steels by advanced powder processing-MIM", J. Advanced Science, 13 (2001) 348-352.

7)   L. Barbe, K. Conlon, B.C. deCooman : "Characterization of the metastable austenite in low-alloy FeCMnSi (TRIP)-aided steel by neutron diffraction", Z.Metallkd., 93 (12) (2002) 1217–1227.

8)   O. Furukimi, K. Maruta, T. Abe, S. Takajo, Y. Habu : "Partially prealloyed steel powder containing nickel and molybdenum for ultrahigh strength sintered materials", J. Powder Metallurgy, 34(3) (1991) 212-214.

9)   O. Furukimi, Y. Saito, N. Makiishi : " Strengthening mechanism of sintered and heat-treated compacts made from partially prealloyed steel powders", Iron & Steel Research Laboratories, Kawasaki Steel Corp., 79 (8) (1993) 1003-1010.

10)   A. Basuki, E. Aernoudt : "Influence of rolling of TRIP steel in the inter-critical region on the stability of retained austenite", J. Mater. Process. Tech., 89–90 (1999)

37–43.

11)   H.K.D.H. Bhadeshia "Developments in martensitic and bainitic steels: Role of the shape deformation", Mat. Sci. Eng. A, 378 (2004) 34–39.

12)   A. Bhattacharyya, G.J. Weng : "An energy criterion for the stress-induced martensitic transformation in a ductile system", J. Mech. Phys. Solids, 42 (1994) 1699–1724.

13)   M. Cherkaoui, M. Berveiller, H. Sabar : "Micromechanical modeling of martensitic transformation-induced plasticity (TRIP) in austenitic single crystals", Int. J. Plasticity,14 (1998) 597–626.

14)   J.M. Diani, D.M. Parks : "Effects of strain state on the kinetics of strain-induced martensite in steels", J. Mech. Phys. Solids, 46(9) (1998) 1613–1635.

15)   Materials Standards for PM Structural Parts, 2009 Edition, MPIF, Princeton, NJ, (2009) 48-49.

16)   Materials Standards for Metal Injection Molded Parts, 2007 Edition, MPIF, Princeton, NJ, (2007) 16-17.

17)   Metals Handbook, 10th ed., vol. 1, ASM Int., Materials Park, OH, (1990) 430-448 and 793-800.

CHAPTER 4

Finite Element Simulation of Heterogeneous Microstructure and Mechanical Properties of Superhigh Strengthening MIM Fe-Ni Steel Compacts

4.1 INTRODUCTION

The compacts fabricated from mixed elemental powder were characterized by heterogeneous microstructure, where various concentration of Ni have been found throughout the compact matrix as confirmed by series of EPMA analysis. The arrangement of various Ni concentrations are referred to as the heterogeneous microstructure. This arrangement is of great importance for the mechanical properties. A good understanding of the role of the microstructure gives great insight into the mechanical behavior of the compact.

In this chapter, the heterogeneous microstructure of the superhigh strengthened Fe-Ni steel compact is highlighted. From experimental work in chapter 3, systematic information of heterogeneous microstructure was obtained. In order to make clear the detailed mechanisms, numerical simulation can be used. Also combination of experimental and numerical works are helpful to understand the mechanisms. Microstructural simulation is the primary interest in this chapter. The models have been constructed by consideration of as much microstructural information as possible from the experimental data.

From careful analysis of the microstructure, two major regions which characterized the compact, were identified; higher Ni region, and lower Ni region (matrix). To verify the experimental data about the roles of these regions in chapter 3, FEM simulations were carried out. The function of these higher and lower Ni regions within the superhigh strengthened Fe-Ni steel compact matrix was deliberately examined. All numerical simulation works in the following sections are predominantly based on these two identified key regions. Taking the TRIP factor into consideration, all FEM simulation models in this study were characterized by a complex network of harder Ni rich martensitic structure and firmly enclosed by tempered martensite. However, in reality a combination of all environmental aspects should be used in the characterization of a material such as part physical shape, size, and working conditions.

4.2 EFFECT OF NI VARIATION ON THE HIGHER NI REGION

4.2.1 Procedure

In this study, the models were prepared to simulate the effect of higher Ni regions on mechanical properties of tempered Fe-Ni steel compact. In order to simplify the real microstructure for FEM, the model was developed based on representative area of Ni element mappings by EPMA analysis. Since the higher Ni regions were about 40 to 50 µm in diameter, a 400×400 µm mapping area was determined as a sufficient representative group of higher Ni regions for modeling as shown in Fig. 4.1.

As illustrated in the left side of Fig. 4.2, higher Ni regions were circled on the EPMA result. In this case, diameter of the circle was 40 to 50 µm, and there were 16 identified higher Ni regions in this area. Further detailed analysis on the Ni element topographies were found that higher Ni regions (inside circle) contained about 6 mass% Ni content and the surrounding matrix (outside circle) contained only 4 mass% of Ni. To simplify the modeling, the 16 circle regions were aligned as shown in the right side of Fig. 4.2. The constructed model was divided into two territories; the higher Ni regions and the matrix.

In order to study the effect of heterogeneity, three different conditions were prepared. Condition 1 was to study the effect of increasing Ni content of higher Ni regions, condition 2 was the simplified model of Fe-6Ni-0.4C fine compacts, and condition 3 was a model without higher Ni regions (homogeneity) as shown in Table 4.1.
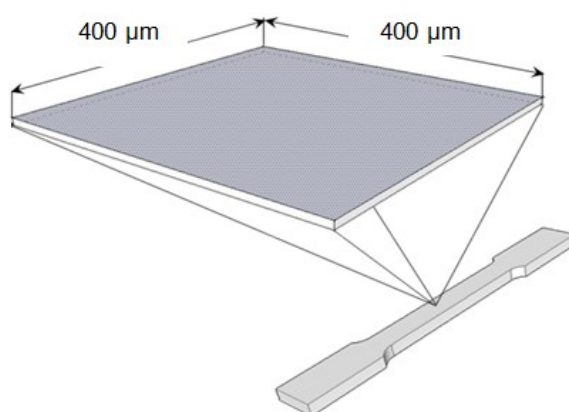

Fig. 4.1 Detailed geometry of micro-scale model.

The workhardening slope for each model was defined as the slope of the stress-plastic strain curve. In this study, the workhardening slopes were developed from our experimental data of three different Ni content by fine Ni powder compacts. The Young's modulus and Poisson's ratio of the model was set to 207 GPa and 0.3 respectively. The Young's modulus value was from the stress-strain curve which experimentally obtained. While, the Poisson's ratio was from a common alloy metal database.

To simulate plane strain behavior, a 2D mesh was implemented throughout the analysis. A 10 % strain was applied at one end of the models in the *y* direction with 200 incremental steps while another end was constrained in the same direction ($u_y = 0$), respectively as shown in Fig. 4.2.

**Table 4.1 Material properties and workhardening rules for model.**

	Matrix	**Higher Ni**
Condition 1 (4×8)	Piecewise linear 4 mass%Ni	Piecewise linear 8 mass%Ni
Condition 2 (4×6)	Piecewise linear 4 mass%Ni	Piecewise linear 6 mass%Ni
Condition 3 (homogeneity-6)	Piecewise linear 6 mass%Ni	
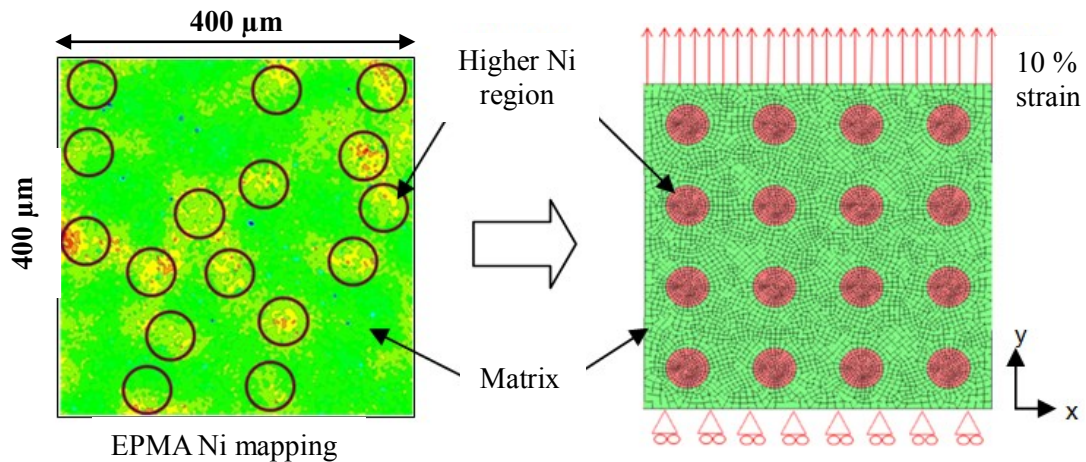
Fig. 4.2 Representative Ni element mapping by EPMA of fine compact and the corresponding model with boundary conditions.

4.2.2 Results and Discussion

Figure 4.3 illustrates the contour plots of equivalent tensile stress σ for the model with condition 1(4×8), condition 2(4×6), and condition 3 (homogeneity-6). The spatial distribution of the higher Ni regions in the model with condition 1 and condition 2 were the same. The only difference between them was the Ni content of the higher Ni regions, where the model with condition 1 offered 2 mass% higher Ni than the model in condition 2. The Ni content for homogeneous model was set to 6 mass% throughout the matrix. More inhomogeneous stress distribution was observed in the heterogeneous state models (condition 1 and condition 2) compared to the model in homogeneous state (condition 3), where the stress was less inhomogeneous. The stress distribution in the three models was very different. This simple comparison shows that the higher Ni regions have great influence on the model predictions.
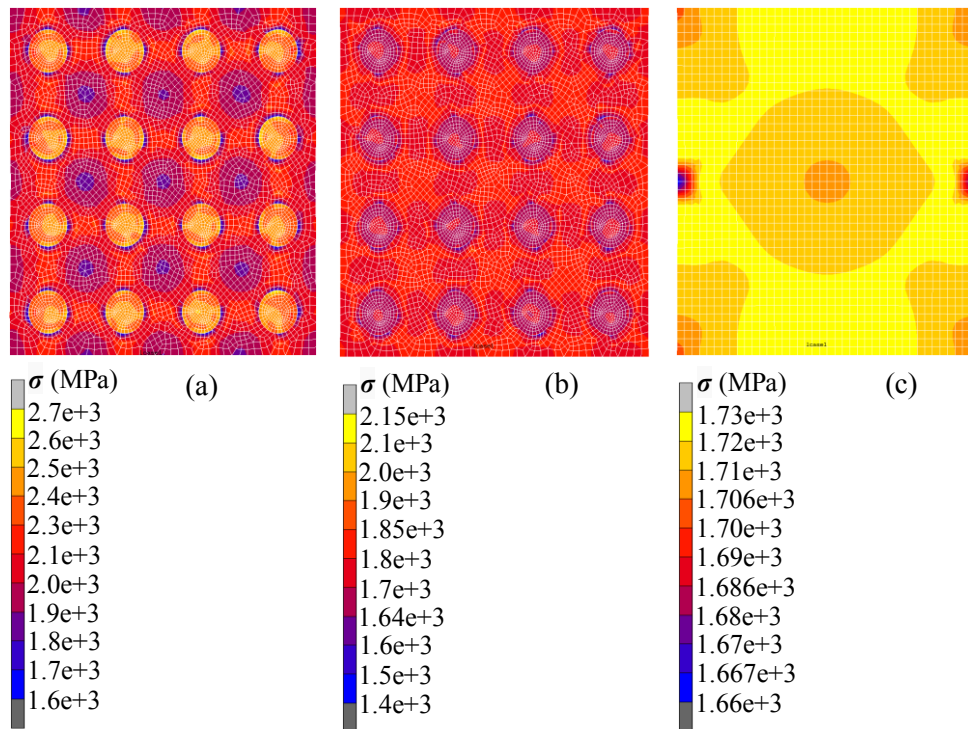
Fig. 4.3 Contour plots of equivalent tensile stress in deformed configuration for

(a) condition 1, (b) condition 2, and (c) condition 3.

The stress was obtained from the center of the model against the strain in the same *y* direction at the end of loading for each model. Note that stress of the heterogeneous models were much higher than that of the homogeneous model, indicated that more load transferred to the higher Ni regions as shown in Fig. 4.3. It is interesting to note that the model with condition 1 which contained higher Ni content in their higher Ni regions predicted best mechanical properties as shown in Fig. 4.4. The model was offered 1910 MPa strength. Followed by the model with condition 2 which offered the strength of 1820 MPa. This can be attributed to the formation of fine heterogeneous distribution of Ni peaks and valleys throughout the steel matrix which strengthened the steel by solid solution effects. The homogeneous model (condition 3) was much weaker than heterogeneous models. The tensile strength was only 1710 MPa.
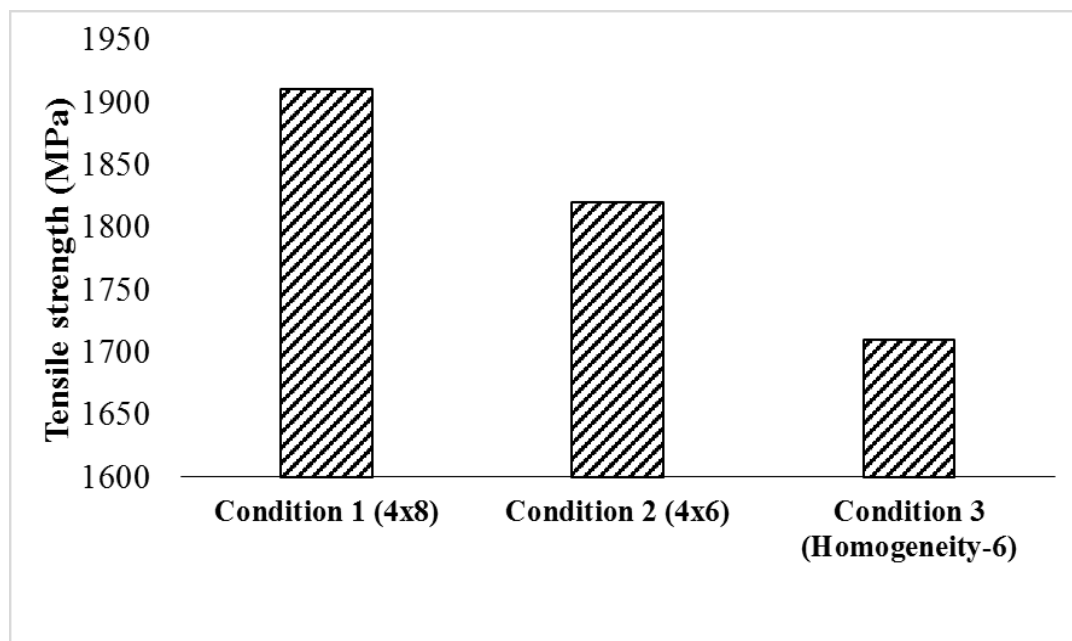
**Fig. 4.4 Simulated tensile stress data with different conditions.**

4.2.3 Summary for Ni Variation Effect on the Higher Ni Region

The stress-strain curve predicted by heterogeneous model showed superior mechanical properties over homogeneous model. The best predicted mechanical properties were obtained by heterogeneous model which contained more Ni content in the regions of higher Ni compared to another heterogeneous model. For that reason, careful control of the dispersion state of the Ni concentration throughout the matrix is a key factor for their excellent properties.
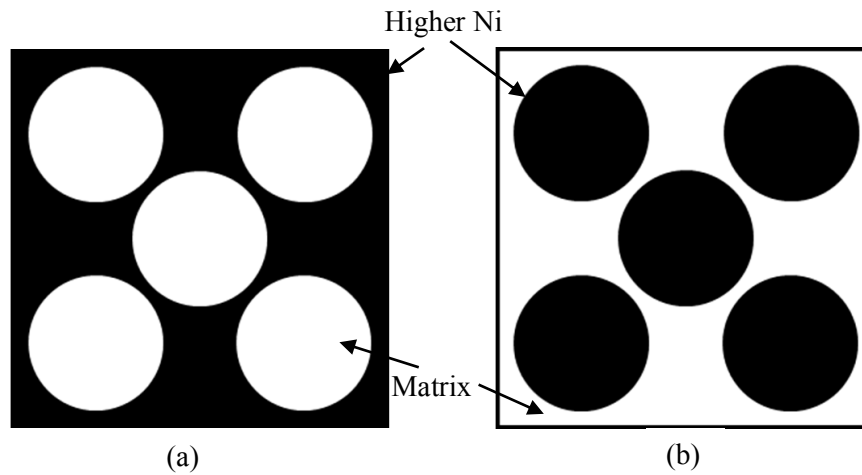
4.3 CONNECTED AND DISCONNECTED HIGHER NI REGION

4.3.1 Procedure

The model was prepared to simulate the effect of connected and disconnected higher Ni regions on the mechanical properties of the compact. The mapping of the higher Ni regions obtained by EPMA analysis could be grouped into two; connected and disconnected as shown in Fig. 4.5. The corresponding FEM models in this study simplified from the EPMA data are shown in Fig. 4.6. In this figure, black region corresponds to the higher Ni area which is defined as the 8 mass% Ni region, while white one as the 4 mass% Ni in the analysis. All constructed model were set by Fe-6Ni-0.4C properties on average.
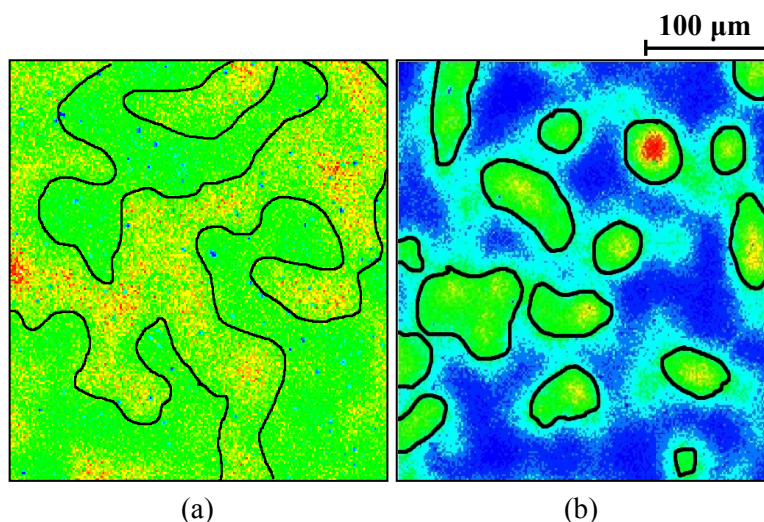
Fig. 4.5 Ni element mapping by EPMA analysis of as-tempered Fe-6Ni-0.4C

compacts (a) connected, (b) disconnected higher Ni regions.

(a) (b)

Fig. 4.6 FEM model contains higher Ni region [black region] network a)

connected, and b) disconnected.

As shown in Table 4.2, four different conditions were prepared. The heterogeneous models of conditions 1, 2, and 3 were contained 5, 9, and 25 individual higher Ni regions, correspondingly. As a homogeneous state, followed by condition 4 connected and disconnected models in each pair were identical in term of outer perimeter, except for arrangements of their individual perfect circle regions. Ni content in each model was kept constant, 6 mass%, therefore by varying the number of individual perfect circle regions from 5 to 25, the size of each one-circle region should be decreasing in order to preserve ratio 50-50 between the higher Ni and the matrix region.

Table 4.2 Designation of the compacts.

Model		Connected Higher Ni Region	Disconnected Higher Ni Region
Heterogeneous	1.	5-con	5-dis
	2.	9-con	9-dis
	3.	25-con	25-dis
Homogeneous	4.	Homogeneous	

The work hardening properties of each model was defined by the stress-strain curves obtained from Chapter 3. The higher Ni region was characterized by Fe-8Ni, whereas the remaining matrix was characterized by Fe-4Ni. The Young's modulus and Poisson's ratio of the model was set to 207 GPa and 0.3, respectively.

A 2D mesh was implemented throughout the analysis. The boundary condition for the present simulation is shown in Fig. 4.7. A displacement was set to simulate tensile testing. Maximum tensile strain was 10 %.
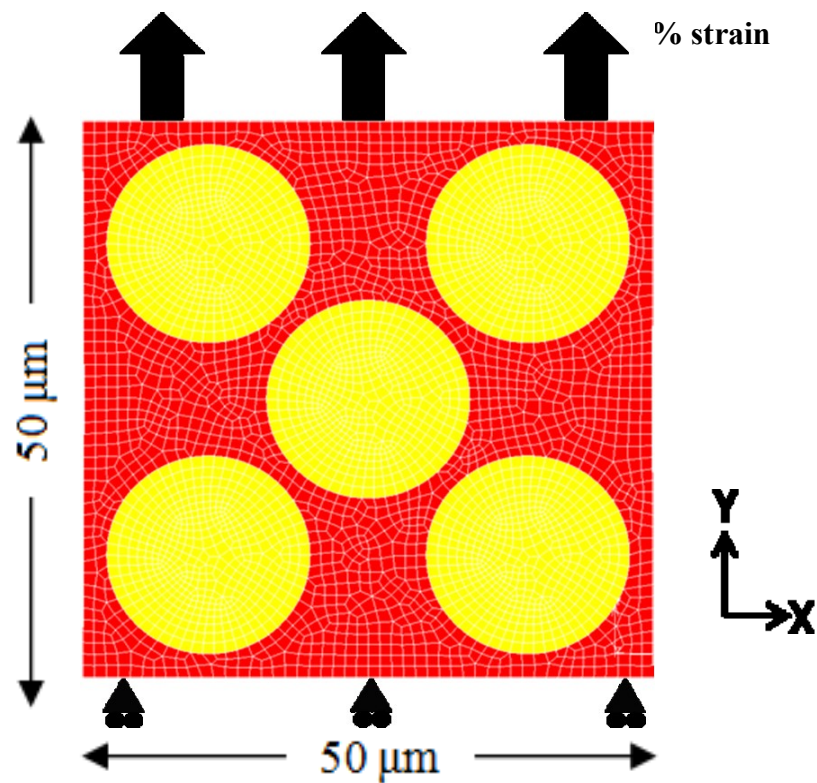

Fig. 4.7 FEM modeling.

4.3.2 Results and Discussion

Figure 4.8 illustrates an equivalent stress σ of the deformed models. The stress distributions in the models of 5-con, 5-dis, 9-con, and 9-dis were almost same regardless different in number and size of the higher Ni regions. Apparently, the stress was found higher on the higher Ni region for both connected and disconnected conditions. Further increased in number and smaller disconnected higher Ni region, less variation of the stress distribution throughout models were observed.

For the homogeneous model, the Ni content was set to 6 mass% throughout the matrix. As shown in Fig. 4.9, the homogeneous model confirmed lowest strength and elongation as compared to the models in heterogeneous state.

In general, the models characterized by the heterogeneous condition were simply outperformed the homogeneous model. Also, note that all connected and smaller higher Ni region models were better performance than disconnected higher Ni regions.

It is worth to note that the model 25-con which contained connected higher Ni regions with smallest diameter of disconnected matrix predicted the best mechanical properties as shown in Fig. 4.9. The model was offered about 2.5 GPa with elongation 10 %, followed by the models of 9-con, 5-con, 25-dis, 5-dis, 9-dis, and homogeneous, consecutively. This can be attributed to the formation of fine heterogeneous distribution throughout models which later strengthen the steel by complicated networks of the higher Ni regions. In this section, the different effects between connected and disconnected higher Ni region models were successfully examined.
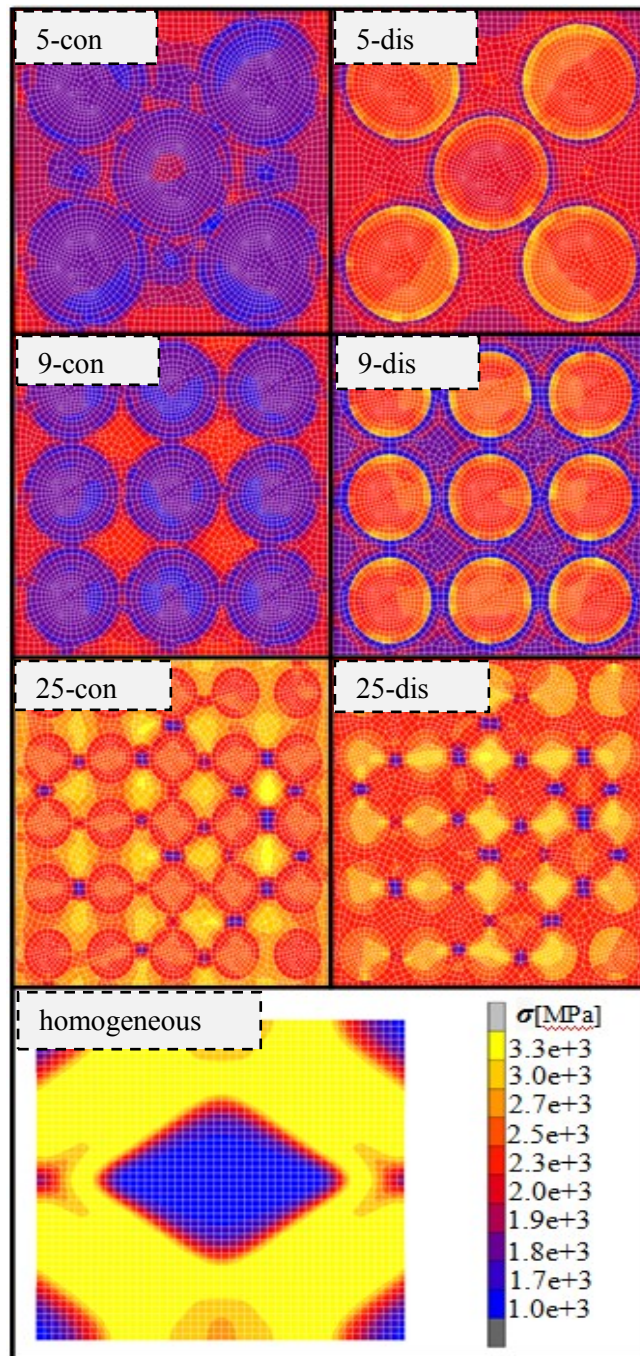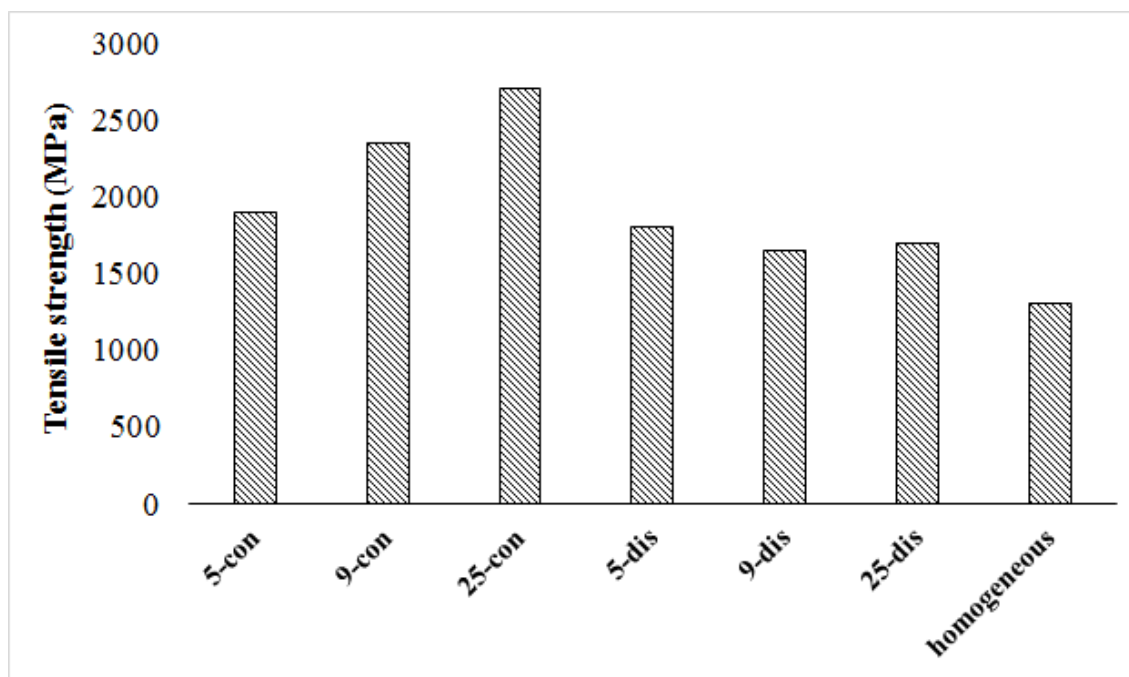
Fig. 4.8 Contour plots of equivalent stress in deformed configuration for all models.

Fig. 4.9 Simulated tensile stress of the FEM models for various conditions.

4.3.3 Summary for Connected and Disconnected Higher Ni Region

The mechanical properties predicted by heterogeneous models confirmed their superiorities over homogeneous model. Also, all models structured as connected higher Ni regions were better performed in their mechanical properties as compared to disconnected one. Furthermore, finer distribution of the higher Ni region was found to be one of possible essential factors in improving their mechanical performance. This was supported by simulated stress-strain curve result which showed a direct relationship between mechanical properties and the size of higher Ni region.

4.4 GRADIENT OF NI CONTENTS

4.4.1 Procedure

In this section, gradient of Ni contents was implemented into the model of heterogeneous microstructure, and mechanical properties were investigated. For the computational approach, five different FEM 2D microstructure models were prepared;

four models represented different heterogeneity, while the other one represented homogeneous microstructure.

The existence of higher Ni region surrounded by matrix region on the Fe-6Ni-0.4C compact using fine Ni powder were obtained experimentally. From detailed Ni element topographies by image analyzing software, average Ni peak in higher Ni region was about 8 mass%. The concentration was gradually decreased from the center of Ni rich area to the matrix region. The concentration reached down to about 4 mass% Ni at surrounded matrix region. Figure 4.10 shows the schematic diagram of single Ni rich area and surrounded matrix region for the Fe-6Ni-0.4C compact using fine Ni powder after heat treatment. While 6 and 8 mass% of Ni content represents the higher Ni region, 4 mass% Ni is for matrix region as model.
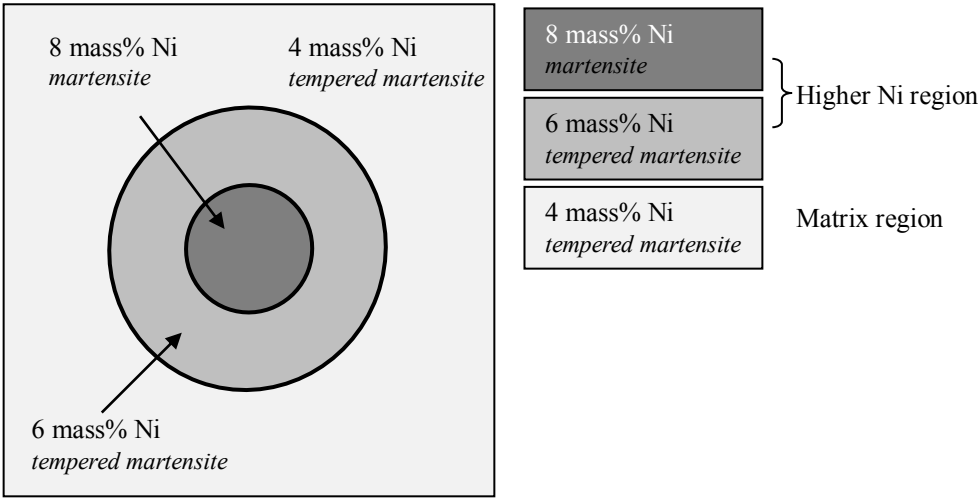
Fig. 4.10 Schematic diagram of multi-regional Ni concentration within the Fe-6Ni-0.4C compact using fine Ni powder.

Averaged size of higher Ni region was found about 40 μm experimentally, therefore 100×100 μm elemental mapping area would sufficient for a satisfactory representative region for the modeling. Full characteristic of these models are summarized in Table 4.3.

Table 4.3 Models condition of the Fe-6Ni-0.4C compacts using fine Ni powder based on the heterogeneous degree.

Model	*Nickel Concentration Region (area %)*			*Heterogeneity (%)*
	8 mass%	**6 mass%**	**4 mass%**	
hetero-100	50	0	50	100
hetero-80	40	20	40	80
hetero-60	30	40	30	60
hetero-40	20	60	20	40
hetero-0 *(homogeneous)*	0	100	0	0

Degree of heterogeneity represents state of Ni diffusivity for each model. High degree means lower diffusion rate so that there is smaller 6 mass% diffused area around 8 mass% region into matrix region (4 mass% Ni). On contrary, when the degree became lower, it indicates better diffusion of Ni element, and bigger 6 mass% Ni area should be represented in the model.

The lowest degree of heterogeneity indicates that the model was fully homogenized where all regions were filled by 6 mass% Ni. When the heterogeneous degree decreased from hetero-100 to hetero-0, area of 8 mass% region decreased from 50 to 0 %, while 6 mass% Ni region increased from 0 to 100 %. These change indicates how much Ni moved out into 4 mass% from 8 mass% Ni region. The experimentally obtained stress-strain curves of homogeneous Fe-4, 6, and 8Ni-0.4C compacts were used as the work hardening inputs for each respective region as shown in Fig. 4.11.
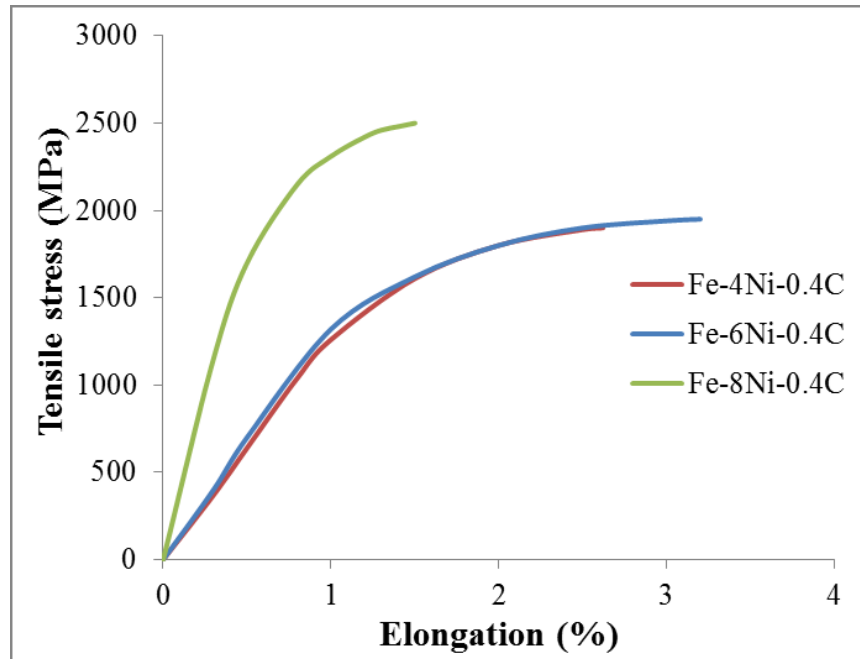
Fig. 4.11 Work hardening curves for the model.

The Young's modulus and Possion's ratio were 210 GPa and 0.31, respectively. Modified hexahedral elements with 8-nodes were used in the elastic-plastic analysis of the model. A typical number of elements in the 2D model was about 4000. Four heterogeneous models and one homogeneous model were prepared as shown in Fig. 4.12. All heterogeneous models consisted of two regions; the higher Ni region (6 and 8 mass%) and the matrix regions (4 mass%).

A 10 % uniaxial strain was applied to all models by fixing the displacement at bottom end in *x* and *y* directions, and applying a uniaxial displacement on top end in the *y* direction as shown in Fig. 4.13.
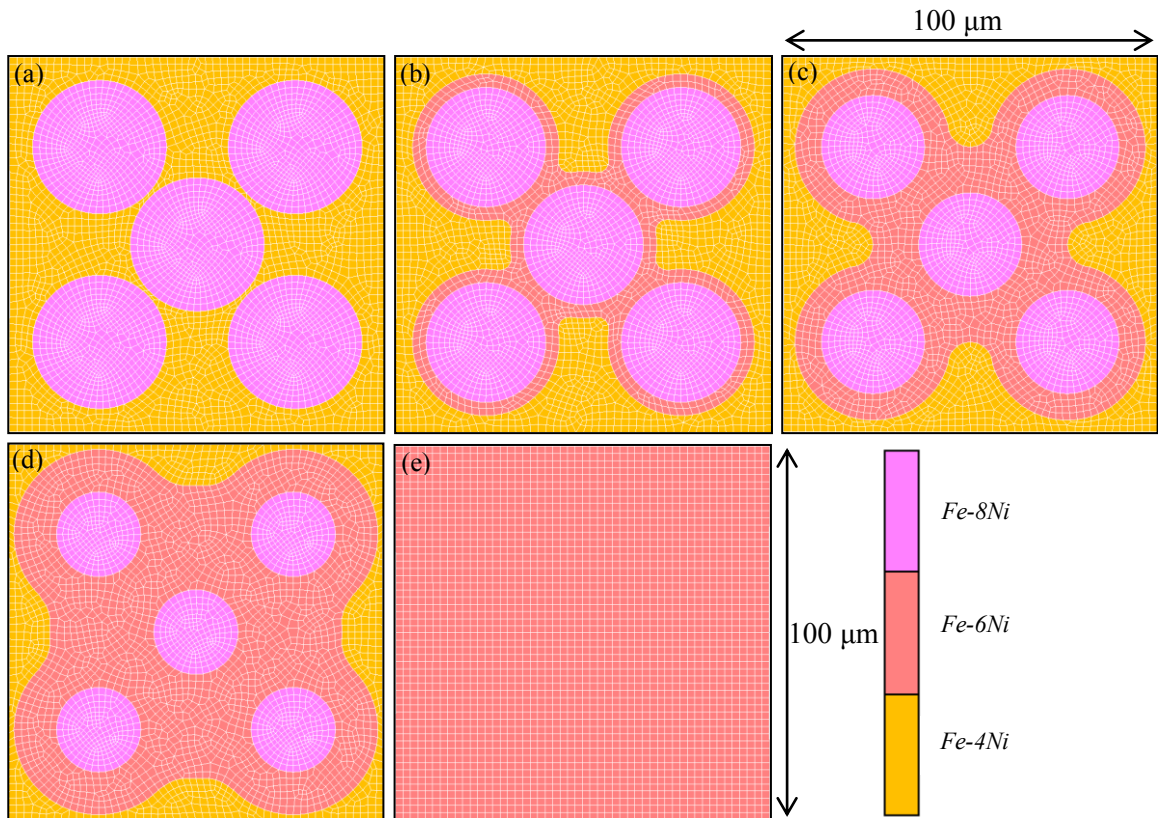
Fig. 4.12 FEM models used in this study. Averaged Ni content of all models were set in the same value of 6 mass%. Each model was named as following; (a) hetero-100, (b) hetero-80, (c) hetero-60, (d) hetero-40, and (e) hetero-0 (homogeneous).
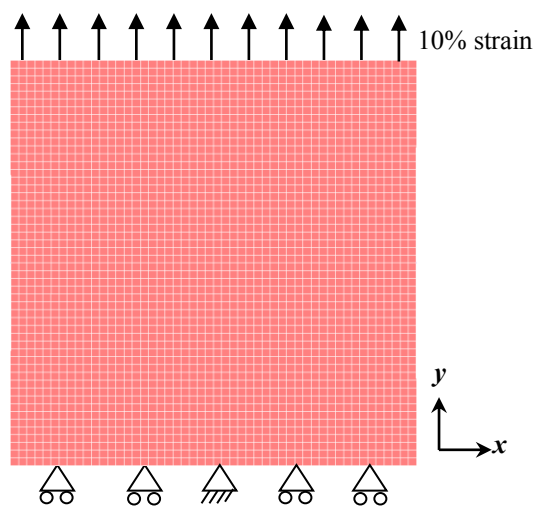
Fig. 4.13 Boundary conditions of all FEM models in this study.

4.4.2 Results and discussion

The distribution of equivalent stress in each of five microstructural models is shown in Fig. 4.14. Note that the higher Ni regions showed much higher stress than matrix regions. Figure 4.14 d) shows a large amount of stress/strain localization took place in the 4 and 6 mass% Ni regions. The plastic strain contours in hetero-40 was quite different, where more inhomogeneous plastic strain was observed. Despite deformation occurred to surrounding 6 and 4 mass% Ni regions, the region of 8 mass% Ni remains relatively intact. This may be explained that 8 mass% Ni, region was responsible to keep the compact stronger while 4 and 6 mass% Ni regions contributed to ductile characteristics.

However, it also might be due to unstable states during simulation works. These results can be confirmed by experimental observations that the solid solution of Ni with fine heterogeneity which consists of Ni rich martensite surrounded by a network of tempered martensitic structure. This heterogeneity resulted in good balance of strength and ductility [2-6].

Conversely, in the homogeneous model (hetero-0), where there was no higher Ni region, the mechanical properties was then solely depends on the attributes of 6 mass% Ni area. The above simulated results are summarized in Fig. 4.15. The advantage of using FEM analysis in the microstructural modeling is that the degree of heterogeneity can be easily modeled to estimate mechanical properties. The presents modeling predicts the experimental behavior quite well; the simulated mechanical properties were improved with the decrease of strong heterogeneity.

Further, the model with 20 % heterogeneity offered the best predicted mechanical properties with strength of 2272 MPa and elongation of 7.7 %. As heterogeneity increased to 50 %, the mechanical behavior also decreased. It is interesting to note that the homogeneous model shows unfavorable result.

However, the analysis presented here showed only qualitative effects of the higher Ni regions on mechanical properties. Therefore, FEM analysis with more complicated

3D microstructure model is underway to obtain a more quantitative description of the mechanical behavior in the Fe-6Ni-0.4C compacts using fine Ni powder.
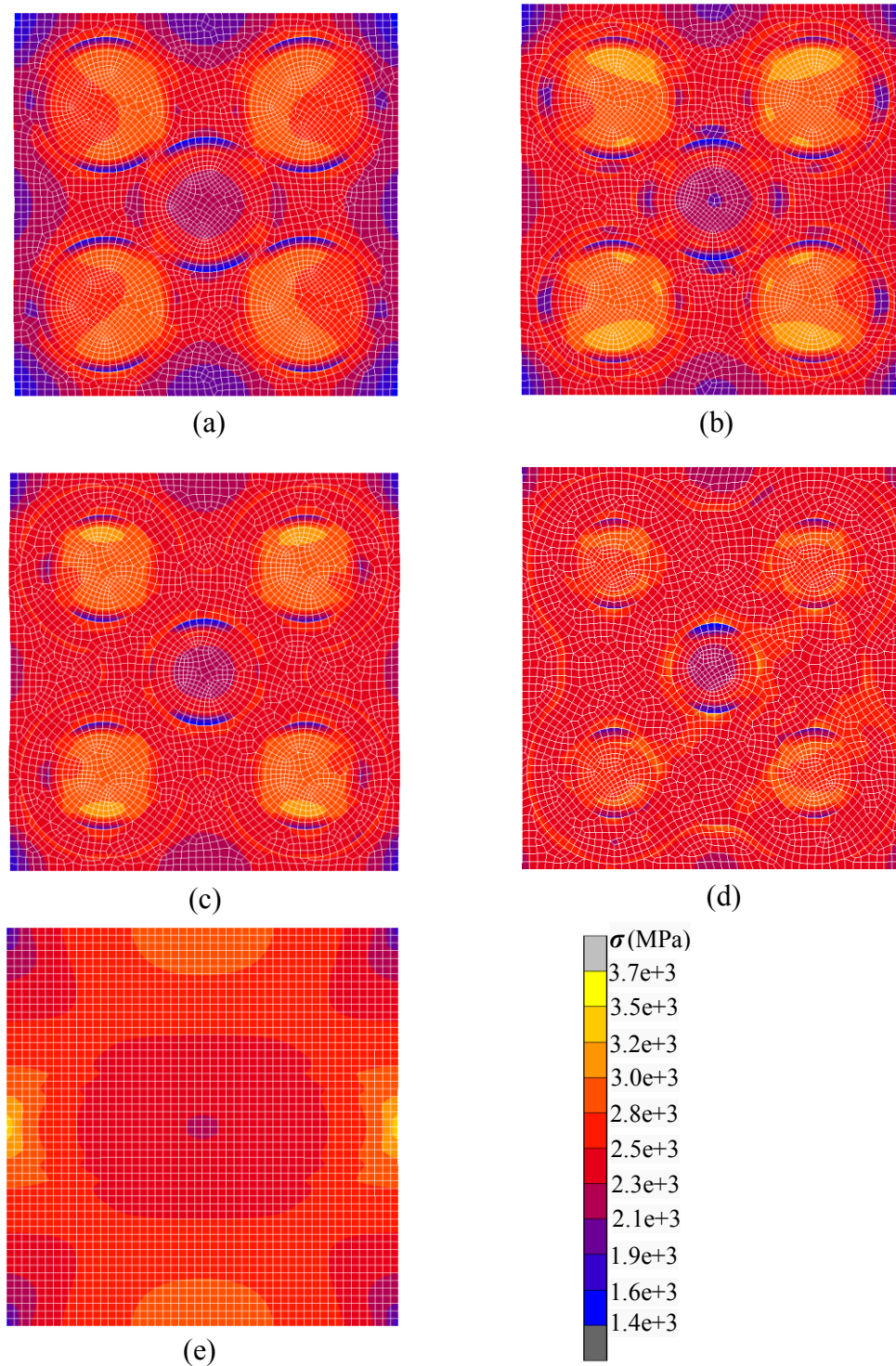
Fig. 4.14 Contour plots of equivalent tensile stress in deformed configuration for (a) hetero-100, (b) hetero-80, (c) hetero-60, (d) hetero-40, and (e) hetero-0 (homogeneous).
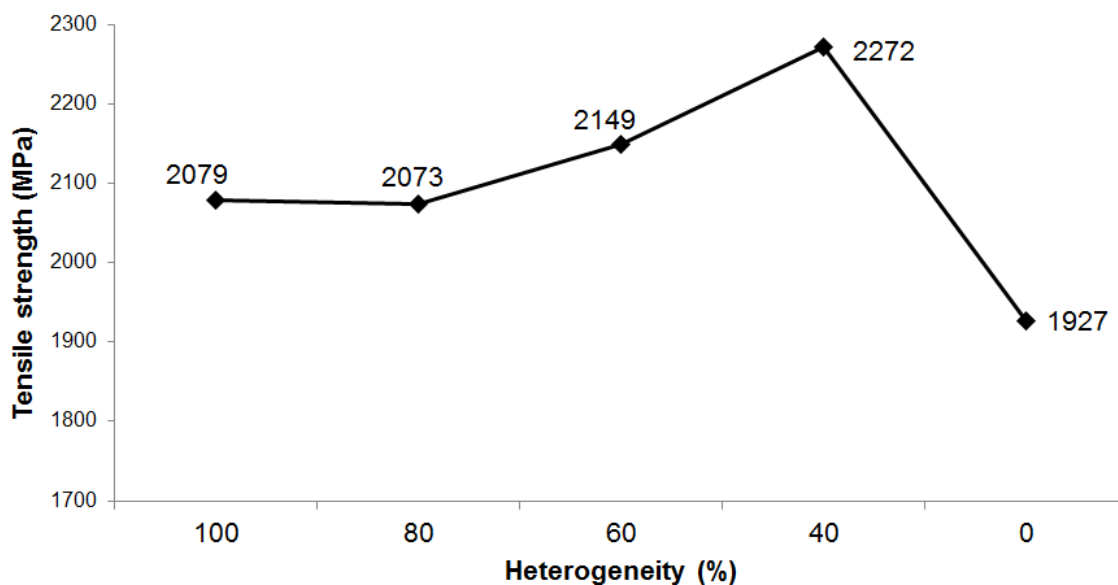
Fig. 4.15 Results of uniaxial deformation simulated by all FEM models.

4.4.3 Summary for Gradient of Ni Content

The effect of heterogeneity on the mechanical properties of tempered Fe-6Ni-0.4C compacts was systematically studied through simulation. Three different regions were introduced into the models in order to wisely represent the Ni gradient phenomena. Fe-8mass%Ni was the region at very center, followed by Fe-6mass%Ni as an intermediate region before all of them being enclosed by Fe-4mass%Ni which known as the matrix region of the model.

When the intermediate region of Fe-6Ni-0.4C appeared in between of the other two regions, the mechanical properties of the model was effectively enhanced. The mechanical properties further improved when the intermediate region was continued to grow. The following conclusions were obtained;

- The state of Ni dispersion throughout matrix is a key factor for their excellent properties.

- Mechanical properties of Fe-6Ni-0.4C compact using fine Ni powder has been improved when optimum heterogeneity (appropriate Ni gradient) was carefully introduced into the model.

4.5 SUMMARY

This chapter was exclusively anticipated on various effects of Ni regions on the mechanical properties of superhigh strengthened Fe-Ni steel compacts through systematic FEM simulation analysis works. The following conclusions can be made based on the results of this study:

1. Simulated heterogeneous model showed superior mechanical properties over homogeneous one. Enhanced predicted mechanical properties were obtained by heterogeneous model which contained relatively more Ni contents in higher Ni regions of compared to another model.

2. FEM models structured by connected higher Ni regions were better performed in their mechanical properties as compared to disconnected one. However, when compared with homogenous microstructure, both of these conditions (connected and disconnected higher Ni regions) were far superior.

3. Finer distribution of the higher Ni region was found to be one of possible essential factors in improving their mechanical performance. This was supported by simulated stress-strain curve result which showed a direct relationship between mechanical properties and the size of higher Ni region.

4. The state of Ni dispersion throughout matrix is a key factor for their excellent properties.

5. Mechanical properties of Fe-6Ni-0.4C compact using fine Ni powder has been improved with optimum heterogeneity in numerical simulation results.

4.6 REFERENCES

1)   YA.YE. Gol'dshteyn and G.A. Charushnikova, "Effect of nickel on cold shortness of steel," Metal Science and Heat Treatment 4 (1962) 497-499.

2)   H. Miura, M. Matsuda : "Ultrahigh strengthening sintered low alloy steels by advanced powder processing-MIM", J. Advanced Science, 13 (2001) 348-352.

3)   H. Miura, M. Matsuda : "Superhigh Strength Metal injection Molded Low Alloy Steels by In Process Microstructural Control", Material Transactions, 43 (2002) 343-347.

4)   M. Matsuda, H. Miura : "Mechanical Properties of Injection Molded Fe-6%Ni-0.4%C Steels with Varying Mo Contents of 0.5 to 2%", Metals and Materials International, 9 (2003) 537-542.

5)   H. Miura : "High Performance Ferrous MIM Components Through Carbon and Microstructural Control",   Materials and Manufacturing Processes, 12 (1997) 641-660.

6)   H. Miura, S. Mitomi, S. Ando, T. Honda : "Effect of homogeneous and heterogeneous structure on the properties of sintered alloy steels by MIM", J. Jpn. Soc. Powder Powder Metallurgy, 42 (1995) 378-382.

CHAPTER 5

Conclusions and Future Directions

5.1 CONCLUSIONS

Investigation of injection molded superhigh strengthened Fe-Ni alloy compacts both experimentally and numerically has been successfully completed. The best obtained mechanical properties by experiment were ultrahigh UTS 2040 MPa, yield strength of 1200 MPa, hardness of 56 HRC, and elongation of 8.1 %.

These excellent mechanical properties were tremendously related to microstructure of the compacts. In this work, FEM modeling for microstructure was employed to evaluate the effect of porosity and the Ni distribution within the microstructural morphology.

At first, high strength 440C stainless steel was selected as a model material to evaluate the effect of pore structure in compact. Since the matrix of 440C is homogeneous, effect of pores could be directly evaluated. In order to examine how these pores effectually inter-react with their mechanical properties, compacts with different porosities were prepared by changing the powder loading.

Higher porosity compact usually characterized by larger, irregular, and highly clustered pores. All of these features are very significant to stress localization, which contribute to premature failure when subjecting to external stresses. Average pore size for the compact at lower porosity were smaller, thus resulted in more homogeneous distribution of stress over larger fraction of the matrix. Tensile properties of 440C steel compact was improved at lower porosity and depreciated when the porosity was higher which was confirmed experimentally and numerically. The pore factor could be eliminated when considering two or more compacts at similar porosity level due to their least effect. However, when the level is varied, then pores abruptly became an important key factor to be completely considered.

As the proposed FEM modeling was useful to check the effect of pores on the mechanical properties, the simulation analysis was enhanced to evaluate the microstructural effect related with Ni distribution. Prior to simulation, three different particle sizes of alloy Ni powders; fine, medium, and coarse, have been systemically

investigated by experimentation work. In all occasions, finer alloy Ni powder always contribute to promotion of better mechanical properties of superhigh strengthened Fe-Ni steel compacts. Tempered Fe-6Ni-0.4C compact with fine mixed elemental powders attained ultrahigh strength of 2040 MPa, with elongation of 8.1 %. The compacts with fine Ni powder were characterized by better diffusivity of Ni element into surrounding matrix as confirmed by EPMA mapping data. Note that, all compacts obtained in this study were heterogeneous-based microstructure.

Besides variation of the Ni content, the presence of a metastable austenitic phase in the microstructure of superhigh strengthened Fe-Ni steel compact has been experimentally identified possibly to be responsible for their good combination of strength-ductility characteristics. Metastable austenitic phase may transform to martensite upon the application of mechanical loading (deformation during tensile testing). In addition to the improvement of the effective strength due to a harder martensitic phase, transformation of retained austenite to martensite is accompanied by relatively large shape and volume changes [1], which induces elasto-plastic deformations in the neighboring region, and generates the so-called transformation-induced plasticity (TRIP) effect.

It is necessary to find out key factors which represent characteristics of the obtained Ni-distributed microstructure. Modeling for numerical simulation should be simplified by considering these factors. As a result, two important regions were systematically identified; the higher Ni, and the surrounding matrix. These two key regions extensively utilized for the FEM simulation analysis in this study. By controlling these two regions, three modelling studies were constructed; a) Effect of Ni variation at higher Ni region, b) Effect of connected and disconnected higher Ni region on the mechanical properties, and c) Effect of gradient Ni content on the mechanical properties. From these modeling, the following results were obtained;

a) **<u>Finer higher Ni region</u>**

The higher Ni region has to be smaller or finer. The smaller Ni-rich regions tend to effectively scattering throughout the matrix of superhigh strengthened Fe-Ni steel compact. As a result, when external stress is applied, more uniform distribution of elastic-plastic stress is found over the compact matrix.

b) **<u>Connected Higher Ni Region</u>**

The region containing higher content of Ni element must be connected to each other in order to form series of strong complicated network. The network acts like a frame to sustain the structure of the matrix when subjected to external stresses.

c) **<u>Gradient of Ni Contents</u>**

Appropriate control of the Ni concentration throughout the matrix is a key to improve the mechanical properties of the Fe-Ni steel compact. Heterogeneous microstructure is a best example, where various concentration of Ni can be found on throughout the compact matrix.

5.2 FUTURE DIRECTIONS

For the future works, there are several possible approached in order to improve the present experimental and numerical works. The present work is a portion of comprehensive foundation for more advance works in the future. Possible future works are briefly explained.

5.2.1 Modeling of Microstructure

The model of higher Ni regions for stress analysis in this study was mainly focused on spherical shape. There are countless of other random shapes to be incorporated to the region of Ni-rich. A comparative studies can be systematically constructed based on these various shapes in order to measure effect on the mechanical properties of the compact.

In this study, there were two interesting regions (the higher and lower Ni region, respectively) have been identified as a key factor to consider for optimizing a complex heterogeneous microstructure of superhigh strengthened Fe-Ni steel compacts. Beside these two, more fundamental factors are expected to be comprehensively explored for better capability to obtain and control an optimum microstructure based on each application in the near future.

5.2.2 Simulation

In this study, the simulation work was conducted in two-dimensional (2D) models. Better representative simulation of superhigh strengthened Fe-Ni steel compact behavior could possibly be obtained by incorporating an actual three-dimensional (3D) microstructure as a basis for the model. "True" Fe-Ni steel morphology orientation and clustering of Ni regions can be incorporated into the model. The 3D microstructure-based FEM will accurately represents the alignment, aspect ratio, and distribution of various Ni concentrations. Therefore, the 3D microstructure-based approached is expected to be more accurate in simulating and understanding macroscopic and microscopic of Fe-Ni steel compact behavior in the future.

The factors of crystalline structures of retained austenite, Ni rich martensite, and tempered martensite are also interesting to be considered. In order to have reliable constitutive model, the mechanically induced transformation and the transformation induced plasticity effects must be incorporated in the model. In many models, the transformation is considered as a function of plastic strain, based on the strain-induced transformation theory. This theory states that the probability of martensite nucleation

sites to transform into a martensite plate is governed by the amount of driving force, both chemical and mechanical, acting on the material [2].

5.2.3 3D Observation

Three-dimensional (3D) microstructure studies of actual microstructure of the compact is useful to evaluate real microstructure. There are several available method for obtaining 3D microstructures, serial sectioning process is one of a basic method [3]. The 2D images from serial sectioning is reconstructed to form 3D virtual microstructure which later can be incorporated into 3D FEM modeling. It should be noted that other techniques, such as X-ray tomography and holotomography have also been employed to the 3D visualization of the microstructure [4-6].

5.3 REFERENCES

1)   D.D. Tjahjanto, S. Turteltaub, A.S.J. Suiker, S. van der Zwaag : "Modelling of the effects of grain orientation on transformation-induced plasticity in multi-phase steels", Modelling Simul. Mater. Sci. Eng., 14 (2006) 617–636.

2)   G.B.Olson and M.Cohen : "A mechanism for the strain-induced nucleation of martensitic transformations", Journal of the Less-Common metals, 28 (1972) 107–118.

3)   N. Chawla, V. Ganesh, B. Wunsch : "Three-Dimensional (3D) Microstructure Visualization and Finite Element Modeling of the Mechanical Behavior of SiC Particle Reinforced Aluminum Composites", Scripta Materialia, 51 (2004) 161-165.

4)   L. Babout, E. Maire, R. Fougeres : "Damage initiation in model metallic materials: X-ray tomography and modelling", Acta Materialia, Vol. 52, Issue 8 (2004) 2475-2487.

5)   A. Borbély, FF. Csikor, S. Zabler, P. Cloetens, H. Biermann :"Three-dimensional characterization of the microstructure of a metal-matrix composite by holotomography", Mater. Sci. Eng., A 367 (2004) 40-50.

6)   P. Kenesei, H. Biermann, A. Borbely : "Structure-property relationship in particle reinforced metal-matrix composites based on holotomography", Scripta Mater., 53 (2005) 787-791.

Dedicated to my beloved wife

Durrani Aimi

and to cherish kids

Altaf Qaisara
Ahmad Mujahid
Aisyah Hani

ACKNOWLEDGMENTS